University of Helsinki
Department of Physics
Master's Degree Program in Physics (M.Sc)

USING THE TIME-DEPENDENT MAGNETO-FRICTIONAL MODEL TO STUDY THE KINEMATIC EMERGENCE OF A TWISTED FLUX ROPE INTO A CORONAL MAGNETIC FIELD ARCADE

Immanuel Christopher Jebaraj

Master's thesis

August 2017

Supervised by

Professor Emilia Kilpua, Ph.D.
Department of Physics, University of Helsinki, Finland

and

Jens A.V. Pomoell, Ph.D.
Department of Physics, University of Helsinki, Finland

HELSINGIN YLIOPISTO
HELSINGFORS UNIVERSITET
UNIVERSITY OF HELSINKI

Tiedekunta/Osasto – Fakultet/Sektion – Faculty	Laitos – Institution – Department
Faculty of Science	Department of Physics

Tekijä – Författare – Author

Immanuel Christopher Jebaraj

Työn nimi – Arbetets titel – Title

Using the time-dependent magneto-frictional model to study the kinematic emergence of a twisted flux rope into a coronal magnetic field arcade

Oppiaine – Läroämne – Subject

Theoretical Physics

Työn laji – Arbetets art – Level	Aika – Datum – Month and year	Sivumäärä– Sidoantal – Number of pages
Master's thesis	September 2017	68

Tiivistelmä – Referat – Abstract

Distinguishing the coronal magnetic field and its evolution can unlock key information on solar energetic eruptions such as the Coronal Mass Ejections (CMEs). CMEs are formed as magnetic flux ropes, i.e. magnetic field lines twisted about each other. They are the main drivers of space weather effects on Earth. Understanding the structure of the internal magnetic field of the CME would help determine the severity of the resulting geomagnetic storm. Predicting the onset and the orientation of the flux rope axis is a major focus of current space weather research.

For this purpose, a numerical study on the kinematic emergence of a twisted flux rope into a coronal magnetic field is performed using the Magneto-frictional method (MFM). The MFM is an exciting prospect as it is sufficiently accurate and computationally inexpensive. The initiation of the eruption is through ideal Magnetohydrodynamic (MHD) kink instability. In this case, the kink instability occurs when the windings of the field lines about the flux rope axis exceeds a critical value.

This thesis presents the set-up of the Fan & Gibson flux rope with different configurations. This was in hopes of studying the slow energization of the coronal field arcade with the emergence of a current carrying flux rope. The results of the simulations presented here show that the several key factors such as the height at which the flux rope is stopped and its twist play a major role in the dynamics of the flux rope in making it kink unstable. One of the main motivations was to use the results to discuss the performance of the MFM in comparison to MHD and how capable it is in capturing ideal MHD phenomenon.

The simulations are also used to investigate the formation of sigmoidal current layer often seen before the onset of eruption. In the results presented here, the sigmoidal "S" shaped current layer is formed as the flux rope becomes kink unstable. This sigmoidal current layer is analysed for different configurations of the flux rope. These results have suggested that accurate dynamic modelling of the coronal magnetic field is essential for successful space weather prediction purposes.

Avainsanat – Nyckelord – Keywords

Plasma Physics, Space weather, Solar physics, Magnetohydrodynamics, Coronal mass ejections, Kink instability, X-Ray sigmoids

Säilytyspaikka – Förvaringställe – Where deposited

Kumpula Campus Library

Muita tietoja – Övriga uppgifter – Additional information

Contents

Chapter 1

Introduction

1.1 The Sun as a star

The Sun is an object of celestial beauty and great fascination and admiration of philosophers, poets and artists. The Sun was conceived from a massive interstellar cloud and this young protostar settled into a state where the plasma and magnetic pressure and the gravitational forces scrambled to balance one another. The plasma was heated by the slow contraction and produced energy. However, through several million years of change and evolution, the Sun has become what it is today. The temperature at its core became high enough for fusion of Hydrogen and Helium to produce energy. It had begun the main phase of its main-sequence life, which would last ten billion years. The sun at present is half way through its life and when it has lived through all its main-sequence life, it will have essentially exhausted its Hydrogen core. However, fusion will continue in what is now a Helium core and this would cause the Sun to expand into a red giant. This stage too will pass and the Sun, which is a Red giant will collapse into a white dwarf the size of earth but with the mass of the Sun. More information about the Sun can be found in several classical books by Priest 1982, Stix 2002 and Aschwanden 2005.

On a cosmic scale, the Sun is a typical main-sequence star of intermediate size and luminosity. It is categorized under the G2 V spectral type with an absolute magnitude of 4.8. However, what makes the Sun special is its close proximity to the Earth. It has a tremendous effect on all living things and also on the space weather(Section 1.2). Studying the Sun is of key importance as it provides a better understanding of other stars and cosmic plasma in general. Some of the important physical properties of the Sun are,

Age:	$= 4.6 \times 10^9$ yrs
Mass ($M_\odot$):	$= 1.99 \times 10^{30}$ kg
Radius ($R_\odot$):	$= 695.5$ Mm ($= 695,500$ km $= 6.955 \times 10^8$ m)
Mean density:	$= 1.4 \times 10^3$ kg m^{-3}
Mean distance from Earth:	$= 1$ AU $= 1.496 \times 10^{11}$ m ($= 215\, R_\odot$)
Mass-loss rate:	10^9 kg s^{-1}
Effective temperature:	5785 K
Equatorial (synodic) rotation period:	26.24 days
Angular momentum:	$= 1.7 \times 10^{41}$ kg m^2 s^{-1}

To put these in perspective, the Sun is about $330,000$ times the mass of the Earth and is roughly 109 times its radius while having a surface gravity which is 27 times stronger. Light from the Sun takes approximately 8 minutes to travel through the 149.6 million kms (1 Astronomical

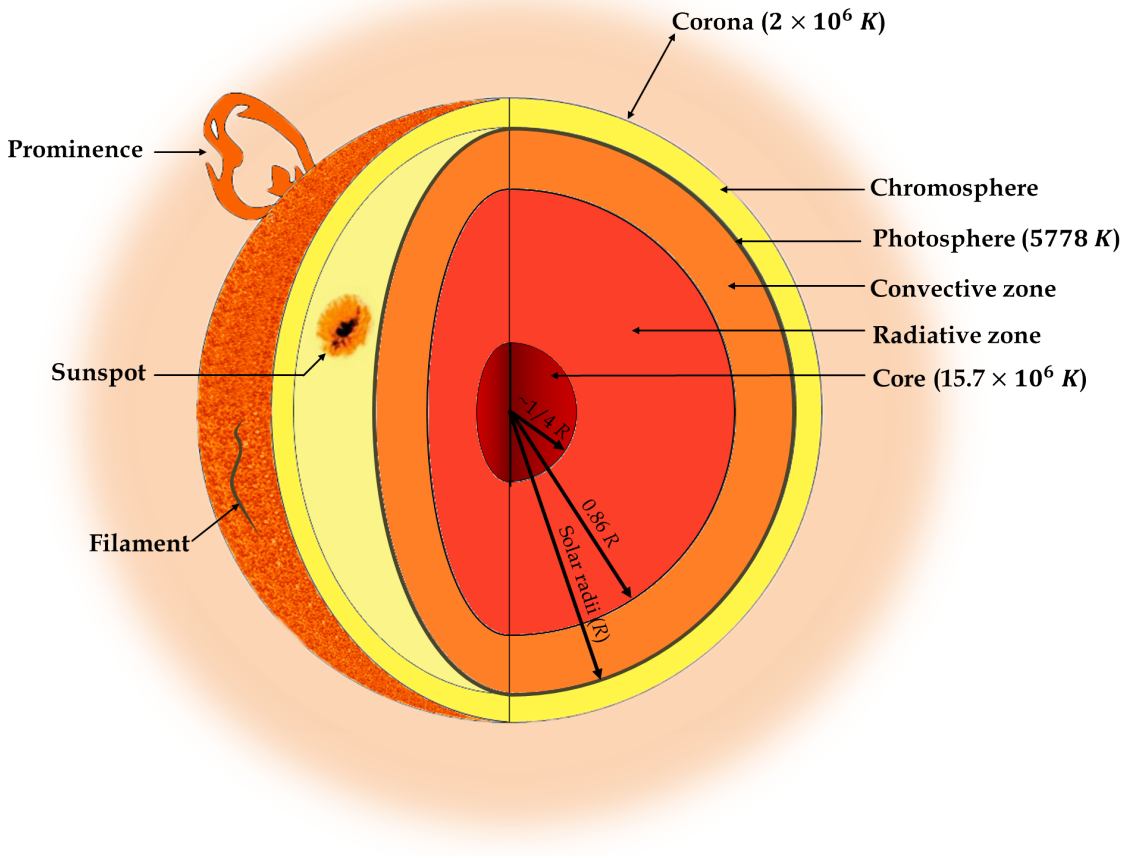

Figure 1.1: Cross section of the Sun indicating the sizes of the various regions and their boundaries and showing several features such as sunspots and filaments.

Unit (AU)).

The 20^{th} century brought along great development in the understanding of the Sun. It became clear that the magnetic fields and the motions of the Sun had a great part to play in the structures being observed and the dynamics being studied. With an increase in observational capabilities and advancements in computational abilities further propelled us towards what is now known as the golden age of scientific discovery. Several structural significances of the Sun such as the sunspots, prominences, flares and coronal mass ejections (CMEs) could be finally seen and studied.

The Sun is a massive ball of plasma (hot ionized gas) that is held together and compressed purely by its own mass and gravity. The Sun is mainly comprised of Hydrogen H(92%) and Helium He(8%) atoms in an ionized state due to the extremely high temperatures. Other minor elements such as Carbon C, Nitrogen N and Oxygen O comprise about 0.1% which is roughly the same proportions as on Earth.

An illustration of the Sun's interior is shown in Figure 1.1. The only layer that is visible to the naked eye is the photosphere. The interior can be divided into three regions, as shown in Figure 1.1, namely the core, radiative zone and the convection zone. These regions are unique and are dominated by different mechanisms which affect each other on the large scale of things. Late in the 19^{th} century, it was found that the Sun's energy through gravitational contractions would only last the so-called Kelvin-Helmholtz time (10^{15} sec $= 3 \times 10^7$ yr). This calculation was done by dividing the gravitational potential energy of the Sun ($M_{\odot}2G/R_{\odot} = 4 \times 10^{41}$ J,

where G is the gravitational constant) by its luminosity at present $L_{\odot} \approx 4 \times 10^{26}$ W.

W. Eddington, in 1925, proposed that the Sun's core was a giant nuclear reactor which would make it last much longer. Since then, models of the solar interior have given a core temperature of 15 million K and a density of 1.6×10^5 kg m^{-3} to make thermonuclear reactions possible. The core temperature is so high that everything exists in a plasma state at a pressure of 230 billion times the sea-level pressure of the Earth. The density too is 13 times that of solid lead. 0.007 kg is converted to energy for every kilogram of Hydrogen (H) that is fused to form Helium (He).

The energy produced in the core through nuclear reactions leak outward through the other layers of the Sun. It is a long process which takes thousands of years before they are released through the photosphere. Since the solar interior is dominated by the plasma forces, it is difficult for the photons to journey to the surface. If the photons have an unobstructed path through the solar interior, they would scale it in 2 sec (at the speed of light). However, it would take the photons thousands of years through it due to the various collisional processes (Mitalas & Sills, 1992).

1.2 Space Weather and solar eruptive events

The Sun is the ultimate source of almost all space weather phenomena. According to the US National Space Weather Program Strategic Plan (Washington DC, 1995), The term space weather refers to the conditions on the Sun and the perturbations it causes in the heliosphere and particularly in near-Earth space. Space weather is important and will continue to be increasingly important as large strides are taken in modern technology. Protecting these technologies in the high atmosphere and in space, as well as on ground, is of utmost importance. Space weather manifests in a number of different ways on Earth. However, the only visible effect is the aurora. All space weather phenomena depend on solar-terrestrial interactions and its main drivers are disturbances in the solar wind and its magnetic field. The space weather effects can also be due to other things from the Sun such as Ultra-violet (UV) and Extreme ultra-violet (EUV), X-rays and solar energetic particles(SEPs)(which are also generated by CME-driven shocks) which are caused by energetic eruptions on the solar surface called the Solar flares.

Coronal Mass Ejections (CMEs) are large-scale eruptive events from the Sun that cause significant disturbances in interplanetary space. CMEs are perhaps the biggest drivers of space weather effects on Earth. CMEs are complex magnetic phenomena and have been subject to a lot of research. The pre-eruptive structures of these CMEs in the corona is the focus of this thesis. They were first identified with OSO-7 (Tousey 1973) and since than have been studied using the on-board coronographs on spacecrafts (Skylab, 1973-74; P78-1, 1979-85; SMM, 1980-89; SoHO, 1995-; STEREO, 2006-present). CMEs can be observed in white light by Thomson scattering of free electrons. They can also be observed in X-rays and EUV. How frequent a CME can occur depends on the solar activity cycle. CMEs are very common during the solar maxima due to the complex nature of the solar magnetic fields. A CME carries enormous amounts of energy (in the range 10^{13} to 10^{15} Wb for axial flux and 10^{14} to 10^{15} Wb for the poloidal flux (Owens, 2008)) and their have kinetic energies typically 10^{22} to 10^{25} J)

Fast shock-driving CMEs are often associated with flares and can accelerate particles to relativistic speeds. These accelerated particles are responsible for the 'snow shower' effect when they hit the CCD detectors on Large Angle and Spectrometric Coronagraph (LASCO) and they are also sources of the largest Solar Energetic Particles (SEPs) events (> 1 MeV) (Yashiro et al. 2004). SEPs are capable of damaging technologies in space and affect astronauts and radio communication.

The interplanetary magnetic field (IMF) as the name suggests, is the Sun's magnetic field in interplanetary space, which is carried out by the solar wind (Smith et al. 1978). The IMF is 'frozen in' to the solar wind plasma that travels outward in a spiral trajectory due to the Sun's rotation (Parker, 1958). The IMF originates from the open magnetic field lines of the Sun, which extend radially into space. The polarities of the fields change with every solar cycle. Being a vector quantity, the IMF has directional components B_x and B_y which are parallel to the ecliptic plane while the B_z component is found perpendicular to the ecliptic plane and is brought about by the solar wind and other disturbances. The IMF B_z when oriented southward, can reconnect with the geomagnetic field lines when they are oriented opposite to each other resulting in a large transfer of energy from the solar wind to the magnetosphere (e.g., Dungey, 1961). Typically, the IMF is weak field with an average value of 6 nT.

Interplanetary Coronal Mass ejections (ICMEs) are defined as transient disturbances in the solar wind that are associated with CMEs. In the literature they are referred to by different names such as ejecta, driver gas, and plasma clouds. ICMEs are massive magnetic structures with typical passage times past a spacecraft in the order of a day (e.g., Klein and Burlaga 1982; Jian et al. 2006). The magnetic field is often significantly enhanced with respect to the solar wind and they have signatures which are distinct from the solar wind plasma they are embedded in (e.g., Zurbuchen & Richardson, 2006). An ICME with a flux rope (Chapter 2) structure is called a magnetic cloud (MC) (Burlaga et al. 1981; Burlaga et al. 1982).

Once a CME is observed, its time of arrival can be estimated by using the measured speed of the CME (e.g., Gopalswamy et al. 2001). On average, it takes 2 to 5 days for a CME to reach the orbit of the Earth after being launched from the Sun depending on its speed and the speed of the surrounding solar wind. In order to predict the strength of an incoming storm, it is important to identify or predict the orientation of the north-south component of the interplanetary magnetic field (IMF) B_z. If the IMF is oriented southward, the incoming magnetic storm could be severe (e.g., Brueckner et al. 1998). The most important current challenges are to predict a CME before it happens and the orientation of the erupting flux rope and its southward IMF.

Although, it is not possible to predict the time of an eruption yet, some indications of the IMF (B_z) orientations can be obtained. On studying the photospheric magnetic field of a CME source region, Marubashi (1997) found that, if it has a bipolar configuration, it is possible to get an idea of inclination of the ICME axis by determining the orientation of the neutral line. Yurchyshyn et al. (2001) found the orientation of the source region of the full-halo CME on Feb 17, 2000 to be in the *north-south* direction, which corresponded to the orientation of the ICME. But since the axial field of the flux rope was oriented northward, there were only very little geomagnetic disturbances. However, the Jul. 14, 2000 halo-CME called the "Bastille day CME" had an *east-west* orientation producing a negative B_z and drove one of the largest storms of Solar Cycle 23.

A number of studies have been made on the flux rope orientations and it is widely accepted that the inclination of the flux rope axes close to the Sun does not have to correspond to the inclination in the heliosphere. For example, the event on May 12, 1997 which had an *north-south* orientation, turned out to be a *south-east-north* (SEN) type orientation instead of the predicted *east-north-west* (ENW) orientation (Webb et al. 2000b) and produced a major geomagnetic storm. Cremades & Bothmer (2004) studied the possible reasons which could be changing these orientations and found that during low activity years, the CMEs are deflected because their inclination is affected by the fast flows from the polar coronal holes. This was further backed up by the February 17, 2000 halo-CME which propagated without the influences from these fast flows from the polar regions because of their absence during the solar maximum. The direction of the magnetic fields in a flux rope CME can greatly affect the eruption and propagation of the ICME. Torok & Kliem (2003), studied the rotation of a flux rope and its dependencies

during its evolution at a coronal level found that rotation can also be due to the flux rope interacting with the neighboring fields. Studies have also found that the rotation of the flux rope is dependent on the flux rope helicity (Chapter 2.2.1) (e.g., Green et al., 2007) and hence, modeling and studying flux rope magnetic properties and these interactions and the resulting instabilities help understand flux rope rotations better and to improve forecasting.

1.3 The Magnetic Sun

The Sun is unique as it still is the only star whose surface can be resolved with current observational technologies. The solar surface can be resolved to a point where the physical processes happening there can be seen in great detail. From these observations, it is now known that the surface of the Sun exhibits several forces and motions and they seem to be causing a vast number of interesting phenomena which are being studied.

The Sun's magnetic field is extremely complex compared to that of the Earth. While the Earth's magnetic field can be described as a dipole, the Sun has multiple poles influencing the atmosphere in many different ways. The magnetic field of the Sun is dependent on the various flows in the solar interior and at its surface. The differential rotation for example, gives the Sun its periods of calm and extreme activity. The indirect manifestation of these magnetic fields are observable in varying wavelengths, from radio waves to X-rays. Direct observations are made using the Zeeman effect through infrared, visible and some measurements of cyclotron radiations at radio wavelength.

1.3.1 Plasma Beta

Before studying the solar magnetic fields in detail, it is necessary to know the relationship between the plasma and the magnetic field. The solar interior and atmosphere exhibit complex plasma and magnetic phenomena, which are either dominated by the plasma or the magnetic pressure. The ratio of these two pressures results in a dimensionless quantity called the plasma β.

$$\beta = \frac{\text{gas pressure}}{\text{magnetic pressure}} = \frac{p}{B^2/2\mu} \tag{1.1}$$

When plasma $\beta > 1$, the gas pressure dominates the magnetic pressure. In the solar atmosphere, this ratio may vary from $\beta > 1$ in the photosphere and at the base of the coronal loops, to $\beta \ll 1$ in the mid-corona, to $\beta > 1$ again towards the upper corona and the heliosphere as the solar wind takes over. Plasma beta provides information about the behavior of a system.

The Sun's interior is normally a very high-β plasma meaning, the magnetic field can be pushed around and stretched and modified by the plasma according to its flow. This is another reason to why motions and flows in the Sun can have such effects on the solar magnetic fields. The magnetic fields can however be considered like unbreakable ropes. They get wound up by the fluid until their strength or energy reaches a point when the magnetic pressure roughly equals to plasma pressure. This interplay between the plasma and the magnetic field pushes the magnetic field lines outward to create various solar magnetic structures. Figure 1.2 is a popular depiction of the plasma - β from the solar interior to the radial flow of solar wind. The region of interest to this work is the $\beta < 1$ region, lower corona.

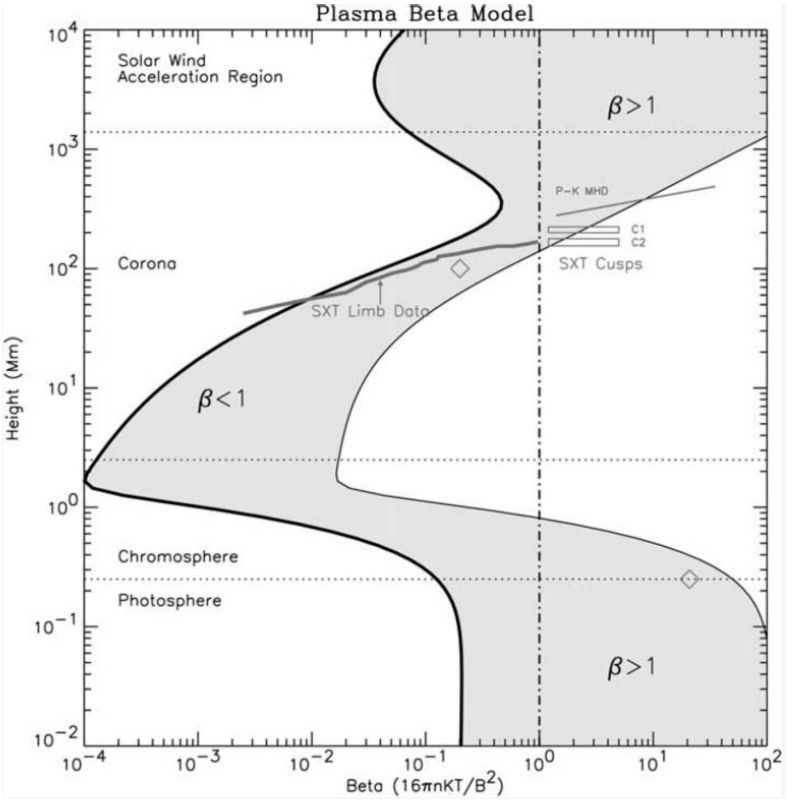

Figure 1.2: Canonical β values for the solar atmosphere. Image adapted from Gary (2001)

1.3.2 Photospheric magnetic field

The photosphere is a thin visible layer on the surface of the Sun and its name comes from the Greek word for 'light'. The photosphere is not uniformly bright and not perfectly still. There are several types of convective motions at work in this region in many different scales. The results of these motions are seen as granulations (Figure 1.3), supergranulations and mesogranulations.

Hale in 1908 found that the photospheric magnetic fields vary greatly in strength. Solanki et al., (2006) studied this further and found that the strongest of them all are the vertical fields (measured in kG). They are found at the boundaries between supergranular cells (Scharmer et al. 2013). The horizontal weaker fields are found in the interior of supergranular cells with field strengths of about 100 to 300 G (Martinez Gonzalez et al. 2008; Borrero, J. M., et al. 2016). There is also the presence of a much weaker ambient field (5 G) in the photosphere.

On a larger scale the photospheric flux is concentrated as intense magnetic flux tubes which have a field strength of about 1 kG and fluxes of 3×10^9 Wb (3×10^{17} Mx) (Stenflo 1973), and these flux tubes are ≈ 100 km in diameter (Solanki et al. 2006). These are regions where the magnetic field is complex and they are called as active regions. Outside these regions of intense magnetic activity, the photosphere is relatively quiet and has a considerably weaker field. However, the flux distribution between the strong and the weak fields in the photosphere is still unclear (de Wijn et al. 2009).

Wide scale flux emergence in the photosphere occurs from the smallest granular magnetic loops (flux as small as 10^9 Wb to flux tubes (10^{12} Wb), supergranular cells (Hassler et al. 1999) and finally, the intense active regions, which can have fluxes in the range is 10^{16} Wb. The active regions unlike the other magnetic phenomena in the photosphere, modify the convection patterns as they appear. The magnetic pressure is intense in these regions and energy escapes into the corona through these regions where the magnetic field dominates.

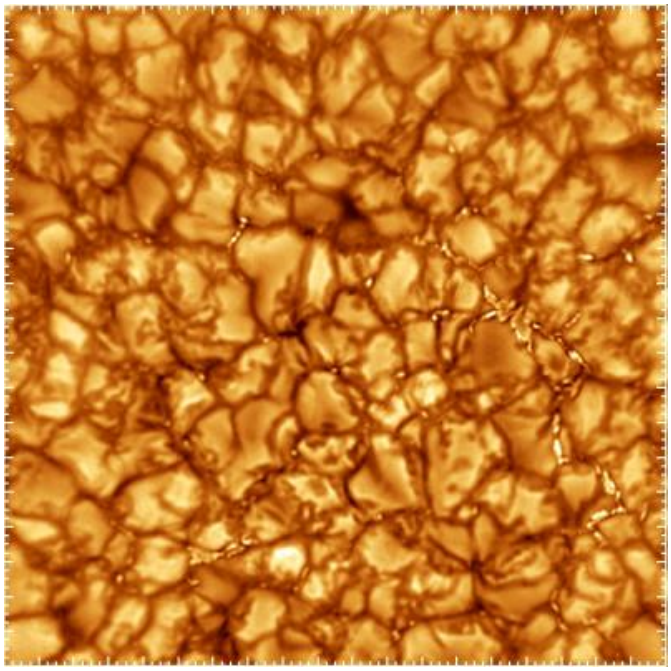

Figure 1.3: A 20Mm x 20Mm field of solar granulation observed in 656.3 nm H – α. Each individual cell is a granule. The dark lanes are the regions between the granules. Credit: BBSO/NJIT

Among other photospheric magnetic structures, active regions are by far the most important for this thesis work. These regions of intense magnetic activity appear when the Sun is active. As mentioned above, active regions have an average magnetic field strength of several hundred Gauss, but there are concentrated regions of flux tubes with much higher field strength, called the sunspots. Sunspot pairs generally appear with an *east-west* orientation with a small tilt so that the leading edge is towards a lower latitude. Their life span is usually several months depending on the sunspot cycle (Trujillo Bueno et al. 2004). Most of the active region flux dissipates due to flux cancellation and submergence; some even spread into the local environment creating unipolar regions (Kuckein et al. 2012), at this stage the active region disappears. Flux transport models are often used to explain the evolution of these large scale photospheric phenomena (Wang & Sheeley 1994; Lin, J., & van Ballegooijen 2005).

Magnetograms are used to observe and measure the magnetic field distribution on the photospheric surface. They are made by combining a narrow band filter with a simple polarimeter. A line of sight(LOS) magnetic field measurement can be made by observing circular polarizations of a magnetically sensitive field line. The measurement can be calibrated to provide magnetic flux density, which is the product of the magnetic field as well as the filling factor (the fraction of the resolution element covered by the line of sight magnetic fields of strength B). Some magnetograms provide only a diagnostic to the LOS component due to their sensitivity to circular polarizations. The Michelson Doppler Imager (MDI, Scherrer et al. 1995) on the SOHO (Solar and Heliospheric Observatory, Domingo et al. 1995) is a widely used magnetograph. The MDI observations have led to an improved understanding of the photospheric magnetic field network (Schrijver et al. 1997). Other diagnostic methods also exists, such as: G-band imagery (qualitative) and the spectro-polarimetric inversions (quantitative) are used in analyzing the magnetic field distribution in the photosphere.

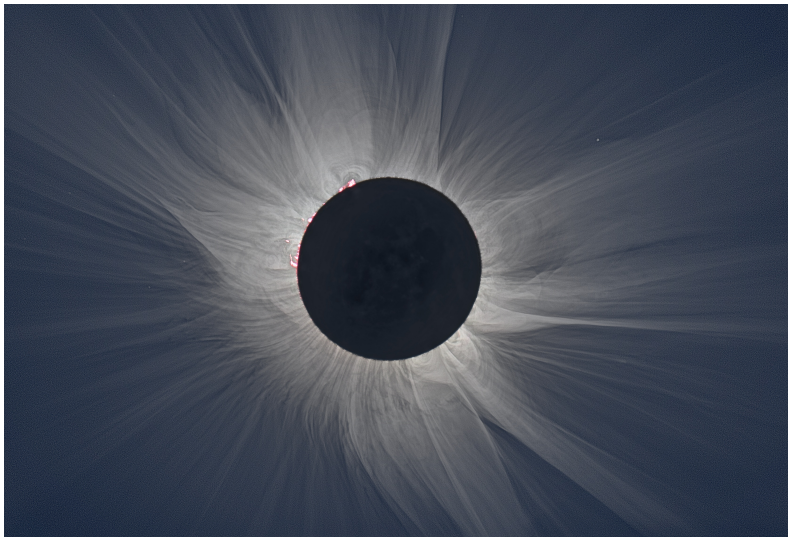

Figure 1.4: A white light image of the solar corona during totality (adapted from NASA; Credits: M. Druckmller)

1.3.3 Coronal magnetic field

The solar corona or the "crown" of the Sun, is a feint halo-like region of extreme temperature (a few $\times 10^6$ K) and is made of very low density plasma. The solar corona is spectacularly visible to the naked eye uniquely during a total eclipse (Figure 1.4). Images of an eclipse showing the solar corona are created by the scattering of light from the photosphere off of electrons (K-Corona) and dust (F-Corona). The corona is brighter when there is more plasma since its brightness is proportional to the electron density. Figure 1.4 shows an image of the corona taken during a total eclipse (*i.e.,* when the Sun is completely covered by the moon). The lines and structures seen there are mostly due to the coronal magnetic fields.

The high temperature of the corona is an active research problem. The corona is hundreds of times hotter than the photosphere. This was realized in 1943 by Swedish astronomer Bengt Edlen. During his studies, the coronal spectra showed a high degree of ionization of the known elements. The temperatures in the corona are high enough for Hydrogen (H) and the heavier nuclei lose electrons allowing for coronal imagining in soft X-ray and EUV.

Direct observation of the solar corona is impossible because of the intense white brightness of the photosphere. However, the corona can be visually observed during total eclipses (Figure 1.4). But these are rare opportunities, which cannot be depended upon if the purpose is to study the corona. In 1930, an artificial eclipse by means of a coronograph was created. A coronograph is a type of telescope with an occulting disc to eliminate the photospheric glare. At present, coronographs are found on-board on two spacecraft (SOHO and STEREO).

The corona can be viewed directly in other wavelengths. For example, soft X-ray telescope are widely used to study corona due to the weak contributions to X-ray from the photosphere and the lower corona. Soft X-ray and EUV observations are done from space since the Earth's atmosphere absorbs these wavelengths. There are a number of satellites, which can image in these wavelengths such as, Yohkoh, TRACE, Skylab, SoHO, Hinode and SDO.

The coronal magnetic field strength varies greatly in magnitude as it typically measures between a few G to several hundred G. The magnetic field strength can be directly measured from radio emissions or through Zeeman splitting(e.g., Lin et al. 2000; Liu & Lin 2008). Most of the current understanding of the coronal magnetic field, however, is largely due to computer models that extrapolate the coronal magnetic fields from the photospheric magnetic field. The magnetic field of the Sun is always a mix of both poloidal and toroidal fields. Even the field-free regions

in between the strong patches of flux have tiny concentration of B. The connection between the field line geometry in the corona depends on how far they have to go to find a region of opposite polarity. The field lines which are not connected are forced out radially as the solar wind (as seen in Figure 1.4) and the dipole like fields get stretched out radially by the plasma ($\beta > 1$).

In the solar corona, the magnetic pressure dominates over the plasma pressure (P) and so the plasma follows the magnetic field lines which means the corona has a very small plasma beta ($\beta \ll 1$). It should be noted that not all parts of the corona have such conditions. The region of interest, the low corona has a plasma flow speed ($u \approx 0$) which can approximate the momentum conservation equation as,

$$-\nabla p + \rho \mathbf{g} + \mathbf{J} \times \mathbf{B} = 0 \tag{1.2}$$

$\mathbf{J} \times \mathbf{B}$ is the most important term in the momentum equation for the solar corona. The pressure and gravitational terms in equation 1.2 balance each other out and the momentum equation can be approximated as,

$$\mathbf{J} \times \mathbf{B} = 0 \tag{1.3}$$

there are two ways to satisfy this approximation, when $\mathbf{J} = 0$ or when $\mathbf{J}$ is parallel to $\mathbf{B}$. The first possible way requires the system to be current-free (although, there can be currents outside the system). This is not a viable approximation as it fails to take into account the presence of current sheets in the corona. The second scenario is when the magnetic fields in the system are in a "force-free" state. Several coronal structures (filaments (Miller et al. 1997), prominences (Lang 1999), and flux tubes) can be approximated to be force-free.

Below the most simple possibility to present coronal fields is presented chosen. Using the approximation in the Ampere's law,

$$\nabla \times \mathbf{B} = \mu_0 \mathbf{J} \tag{1.4}$$

when $\mathbf{J} = 0$,

$$\nabla \times \mathbf{B} = 0 \tag{1.5}$$

this magnetic field can be expressed as a gradient of the scalar potential function,

$$\mathbf{B} = -\nabla \Psi \tag{1.6}$$

This gives a minimum energy state for the magnetic field called the potential field. Adding a non-zero $\mathbf{J}$ to equation 1.4, be it in terms of twist or some form of energy, forces the system to lose its potential state marking a build up in the total magnetic energy in the field. A potential energy state is used as an initial condition for the coronal magnetic field in the numerical study presented in Chapter 4.

Chapter 2

Magnetic Flux ropes

Magnetic flux ropes (FR) are a major topic in the study of the solar corona and space weather. The corona is usually considered to be in a force-free equilibrium. Magnetic flux ropes (FR) can be defined as a set of magnetic field lines wrapped around an axial field line. They are energetic structures that release their stored energy in the form of an eruption (CME, flare, etc.,). To understand these eruptive phenomena as well as predict their onset, it is necessary to investigate the structures in the corona, their underlying dynamics, and the build up of energy that causes these massive eruptions. It is also important to study the physical mechanisms that could trigger these explosive releases of energy.

A brief description of the coronal magnetic field can be found in Chapter 1.3.3. The background corona is often approximated to be in a potential or "ground" (lowest energy) state. However, there needs to be sufficient amounts of free energy for an onset of an eruption. By introducing a twisted magnetic flux rope into the corona, the coronal magnetic fields lose their equilibrium and get energized by the flux rope (Forbes & Isenberg 1991). There are two dominant theories about the loss of equilibrium in the solar corona and they are the helical kink instability (Anzer 1968), and the torus instability (Bateman 1978). A description of these mechanisms can be found in Chapter 2.3.1 and 2.3.2.

2.1 Flux rope formation

Several theories on how FRs form have been put forth (Rust and Kumar 1994; Priest et al. 1996; Kuperus 1996; Kuijpers 1997; Zirker et al. 1997, etc.,). FRs can either be formed before or after an eruptive event. The flux rope emergence model assumes that a pre-existing FR emerges into the corona due to convective instabilities (Fan 2001, 2010; Manchester et al. 2004a, 2004b; Magara 2006). The flux cancellation model is another model that suggests that reconnection of magnetic field lines due to the shearing motions creates an FR(van Ballegooijen & Martens (1989)).

The work presented in this thesis is based on Fan & Gibson (2004) which considers a pre-existing flux rope that is driven into the corona. In the Fan & Gibson (2004) model, the FR is driven through the convection zone due to the magnetic buoyancy instability (Moreno-Insertis 1997).

Figure 2.1 shows a twisted current-carrying FR in the convection zone. Confined(current-carrying) FRs posses neutralized currents (e.g., Parker 1996), which means that the total current, $\mathbf{J}$, when integrated over the FR magnetic polarity, vanishes. This would mean that the main current flowing through the FR which connects the FR polarities is surrounded by a return

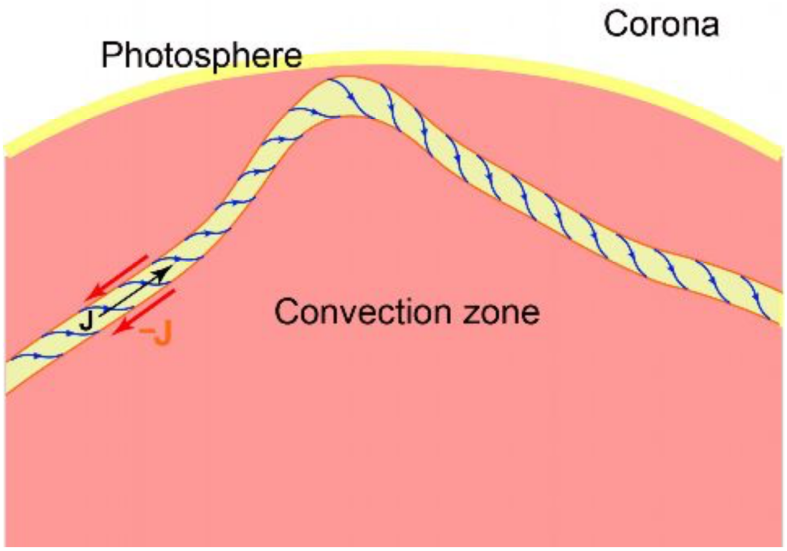

Figure 2.1: Emergence of a twisted flux rope from the convective zone (adapted from Filippov et al. 2015).

current(opposing current) of equal strength. The FR is bound by this opposing current and held in place by the plasma pressure (Parker 1979). Once the FR emerges into the corona, the opposing current spreads out across the photosphere. Observations made by the Solar Optical Telescope(SOT) on board Hinode have indicated emergence of FR into the corona along the polarity inversion line (PIL). This was analyzed e.g., by Okamoto et al (2008, 2009) who suggest the emergence of helical flux in order to keep the prominence active. This was later confirmed by Lites et al. 2010 for twisted FRs.

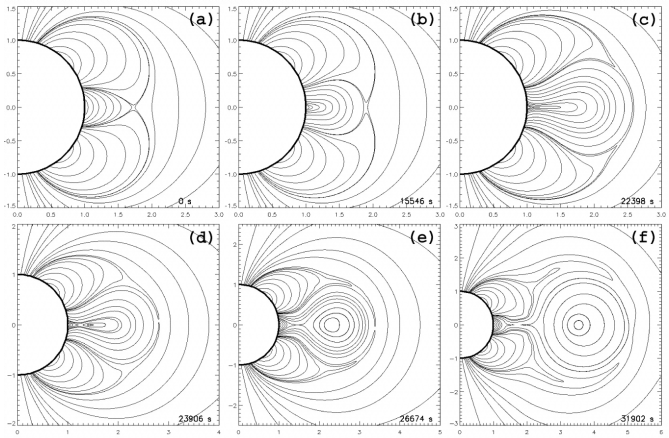

Figure 2.2: Meridional projections of magnetic field lines throughout the magnetic breakout eruption process at six different times. (a) shows the initial potential state with the four flux system. (c) shows the overlying flux transfered to the side arcades. (e) shows a rapid magnetic release and (f) shows the rebuilding of the shear arcades after the flux is squeezed out. (credits: Lynch et al. 2004)

In some other models, the FR is formed as a consequence to the eruption through flare reconnection. Antiochos et al. (1999) proposed a model where the flux in between sheared arcades is squeezed out forming a current sheet. This forces reconnection of the sheared side arcades forming an FR which erupts. Figure 2.2 shows an illustration of this model, called the breakout reconnection model. It has been found to have caused major CME events (e.g., Aulanier et al. 2000). Another model with a similar mechanism is the tether-cutting model (Moore et al. 2001). In this model, a flux rope is formed during the onset of eruption when sheared arcades reconnect below the flux rope to form a twisted loop.

Most of the above mentioned FR formation scenarios have one common mechanism: reconnection. Magnetic reconnection plays a key role in releasing the excessive magnetic energy that is built up and stored in the magnetic field (e.g., Berger & Field 1984). Magnetic reconnection occurs when oppositely directed magnetic field lines in a plasma break and reconnect. The main feature of this phenomena is the huge release of energy that was previously stored in the magnetic field. The magnetic energy is converted to kinetic energy and heat. Reconnection was first theoretically described by Parker (1957) and Sweet (1958) and since then has been at the core of solar physics. Magnetic reconnection implies that the violation of the ideal MHD condition where magnetic field lines are "frozen-in" to an infinitely conducting plasma, i.e., charged particles which are on circular orbits around the magnetic field lines and do not diffuse and mix. When oppositely directed field lines are squeezed together, a thin current sheet is formed and when plasma diffuses, there is magnetic reconnection. For the plasma to diffuse, there must be finite conductivity that allows even the smallest amount of resistivity. A detailed description of magnetic reconnection can be found in a number of textbooks.

2.2 Magnetic Helicity

To put it in the simplest possible way, magnetic helicity is the measure of complexity in a closed volume of magnetic field lines and is a conserved quantity. It can be thought of as a swirl in the magnetic field. Magnetic helicity plays a key role in discussions involving flux ropes and instabilities. Taylor (1974) revealed that magnetic helicity in laboratory plasmas are conserved when they dissipate and spread uniformly through reconnection. Based on Taylor's analysis, Heyvaerts & Priest (1984) described solar conditions implying that any changes to the force-free coronal magnetic field is due to magnetic helicity.

The transfer of helicity into the solar corona from the Sun's interior (Low 1994) because of the dynamo (Chui & Moffatt 1995) is a widely accepted explanation for the complex nature of the coronal magnetic field during solar maxima. Rust & Kumar (1994) proposed the concept of "helicity charging" by which the helicity is transported to the corona (and coronal structures) from the photosphere. On how it could be done was a subject of debate and it was suggested that the photospheric shearing motions twist and untwist magnetic flux while building up energy along those field lines which are later shed through eruptive events (Low 1996).

A detailed description of magnetic helicity can be found in Priest (1982, 2014) or Aschwanden (2005). However, a brief understanding of helicity is as follows:

The vector potential $\mathbf{A}$ is used in describing magnetic helicity (H). It is possible to choose a gauge with freedom for a given potential function (in this case $\mathbf{A}$). The magnetic field $\mathbf{B}$ can be written in terms of the vector potential as,

$$\mathbf{B} = \nabla \times \mathbf{A} \tag{2.1}$$

$\mathbf{B}$ does not change with the gradient of a scalar field (ϕ) to $\mathbf{A}$

$$\mathbf{B}^* = \nabla \times (\mathbf{A} + \nabla\phi) = \nabla \times \mathbf{A} = \mathbf{B} \tag{2.2}$$

$\mathbf{B}^* = \mathbf{B}$ which means, $\nabla \times \nabla\phi = 0$. With gauge variance, it is possible to change the Coulomb gauge ($\nabla \cdot \mathbf{A} = 0$) and magnetic helicity,

$$\mathbf{A} \cdot \mathbf{B} = \mathbf{A} \cdot \mathbf{B} + \nabla\phi \cdot \mathbf{B} \tag{2.3}$$

This would also mean that the gauge dependence applies to the total helicity as well,

$$\int_{\mathrm{V}} \mathbf{A} \cdot \mathbf{B}\, \mathrm{dV} \rightarrow \int_{\mathrm{V}} \mathbf{A} \cdot \mathbf{B}\, \mathrm{dV} + \int_{\mathrm{V}} \nabla\phi \cdot \mathbf{B}\, \mathrm{dV}, \tag{2.4}$$

$$\mathrm{H} = \int_{\mathrm{V}} \mathbf{A} \cdot \mathbf{B}\, \mathrm{dV} + \int_{\mathrm{S}} \phi \mathbf{B} \cdot \mathbf{n} \mathrm{dS}, \tag{2.5}$$

where $\mathbf{n}$ is the unit normal to the surface S point out of the volume V.

By applying the Gauss divergence theorem to Equation 2.4 transforms it from a volume integral to a surface integral with surface normal (S) resulting in Equation 2.5 for helicity.

Berger & Field (1984) pointed out a gauge invariant version of magnetic helicity, known as the relative helicity,

$$\mathrm{H_R} = \int_{\mathrm{V}} (\mathbf{A} + \mathbf{A}_\mathrm{r}) \cdot (\mathbf{B} - \mathbf{B}_\mathrm{r})\, \mathrm{dV} \tag{2.6}$$

It is relative to $\mathbf{B}_\mathrm{r} = \nabla \times \mathbf{A}_\mathrm{r}$ and $\mathbf{B}_\mathrm{r} = \nabla\phi_\mathrm{r}$ with a boundary condition $\mathbf{n} \cdot \mathbf{B}_\mathrm{r} = \mathbf{n} \cdot \mathbf{B}$, with $\mathbf{n}$ being the normal vector to the surface.

Moffatt (1969) interpreted magnetic helicity as mutual linkage between magnetic field lines. Mutual linkage is directly proportional to the magnetic helicity and is the number of times magnetic field lines are linked with each other. It is given as,

$$\mathrm{H_M} = \int_{\mathrm{V}} \mathbf{A} \cdot \mathbf{B}\, \mathrm{dV} = 2\mathrm{n}\, \phi_1 \phi_2 \tag{2.7}$$

here, n is the mutual linkage number and ϕ_1 and ϕ_2 are the magnetic fluxes of the field lines being linked.

Moffatt & Ricca (1992) prove that for a knotted flux rope with flux ϕ, the invariance of helicity (H) with flux conservation is equal to the sum of writhe and twist. The twist (T) can be defined as the number of field line turns about the flux rope axis and the writhe (W) can be defined as the number of times the flux rope axis winds itself (self helicity)(Berger 1999; Rust 2002).

$$\mathrm{H} = \mathrm{h}\phi^2 \tag{2.8}$$

$$\mathrm{h} = \mathrm{T} + \mathrm{W} \tag{2.9}$$

Since helicity is a conserved quantity, twisted flux ropes often convert writhe to twist which can mark the onset of the helical kink instability (Torok & Kliem 2005). There have been discussions on whether helicity could be transferred between different parts of the prominence when the helicity(H) is conserved (House & Berger 1987).

2.3 Flux rope eruptions

Flux ropes are key for understanding the eruptive phenomena at the Sun such as CMEs. However, many questions about how they erupt and the occurrence of reconnection still remain. Ji et al. (2003) observed that some eruptions are confined and fail to lead to a CME. These so-called "failed eruptions" have been observed several times since then (e.g., Guo et al. 2010a). Flux ropes are equilibrium structures which erupt when they lose that equilibrium or stability (Bateman 1978). Several theories have been suggested for this loss of stability.

There are a number of great textbooks which describe flux rope stability (e.g: Boyd & Sanderson 2003; Goedbloed & Poedts 2004) in detail. The general consensus is that instability-driven FR eruptions occur when the threshold for stability is exceeded. Since FRs are described in the corona using magnetohydrodynamic (MHD), it is necessary to look at their eruptive mechanisms from an MHD perspective. As discussed briefly in Chapter 1.3.3, the coronal magnetic field exists in a potential state for the most part and is current free. The time scales of eruptive events is too small to consider changes in the photosphere. This suggests that at the time of eruption, the solar coronal magnetic fields contain large amounts of free energy. FRs carry a current that develops further as they accumulate through a constant transportation of flux into the corona. Once the corona has accumulated enough energy, the eruption is triggered violently due to a loss in equilibrium between the upward pressure and downward tension (Janvier et al. 2013). This is believed to be the basic mechanism behind solar eruptions (see also Forbes et al. 2006). In their review, Schmeider et al. (2004) explain in detail with observations about different possible mechanisms which could occur during the eruptive phase. There are several eruptive models presented in the literature, which partly share similar results and mechanism and are hence difficult to differentiate.

Fan & Gibson (2004) put forward an eruption model using MHD where they inject electric current in the form of a flux rope into the corona. This is done by allowing a twisted flux rope to emerge through the photosphere into the corona while utilizing a coronal field arcade energized by the flux and becoming non-potential during the eruption phase. The flux transport leading to flux build up and to the eruption phase is achieved via a time-dependent bottom boundary. Fan & Gibson have utilized this model in several of their consequent studies (Fan 2005; Fan & Gibson 2007).

2.4 Flux Rope Instabilities

The basis for instability is understood from the energy diagram shown in Figure 2.3. This suggests that a confined structure does not have to be necessarily stable since it is in equilibrium. The confinement could be that of a ball on a hill requires only a small perturbation to be unstable. An equilibrium is always unstable when the potential surface (curvature of the surface in Figure 2.3) is located downward from the equilibrium location.

As discussed in section 2.3, the stability of the flux rope plays a key role in solar eruptions (van Tend & Kuperus 1978; van Tend 1979). The loss of stability in a current carrying flux rope can happen either by exceeding the threshold for twist or height (Bateman 1978; Rust & Kumar 1996; Torok & Kliem 2005). Shafranov (1966) suggested that for a flux rope carrying a current, the external poloidal field creates a pinch due to a toroidal current, and therefore the flux rope is balanced by Lorentz forces applied upwards (Kuperus & Raadu 1974) through the coronal flux and downwards externally by the poloidal field. This balance can be broken at any point due to an excessive build up of magnetic energy or helicity and result in instability.

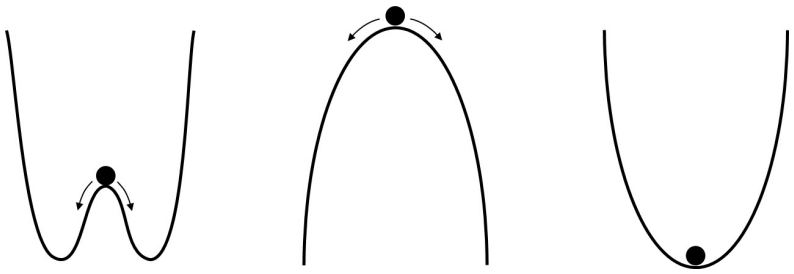

Figure 2.3: An energy diagram of the potential energy surface. (*left*) system in equilibrium but still unstable because of a downward curvature of the potential energy surface, (*middle*) a system in a non-equilibrium state and hence highly unstable, (*right*) a system which is highly stable and in equilibrium because it exists in the lowest point of the potential energy surface.

When considering the stability of a toroidal flux rope, the internal and the external forces must be in equilibrium. Recent studies (Torok & Kliem 2005; Fan & Gibson 2004) have shown that two ideal MHD instabilities, namely the torus instability (TI) and the helical kink instability (KI) are important in solar eruptions. Both KI and TI are briefly described below play key roles in this thesis.

2.4.1 Torus Instability

Current understanding of the torus instability in solar flux ropes was proposed by Torok & Kliem (2006). The interpretation was based on the idea of a tokamak instability which, in turn, was suggested by Bateman (1978). Their study was based on an interest in the expansion of current carrying FRs found in space plasma (Forbes 2000). Grad & Shafranov (1958) developed the equilibrium conditions for a flux rope with torus geometry by connecting the two ends of a cylinder together. However, by doing this, the newly formed toroidal structure loses its equilibrium. There is an outward expansion due to the pressure force inside the torus pushing outward. Another reason is the current that flows through the torus is anti-parallel (opposing Lorentz force) resulting in the expansion in the major axis of the torus. An external poloidal field is necessary for the system to attain equilibrium. In a tokamak, this is done so by controlling the external fields to maintain equilibrium; However, it is not the case for the solar corona.

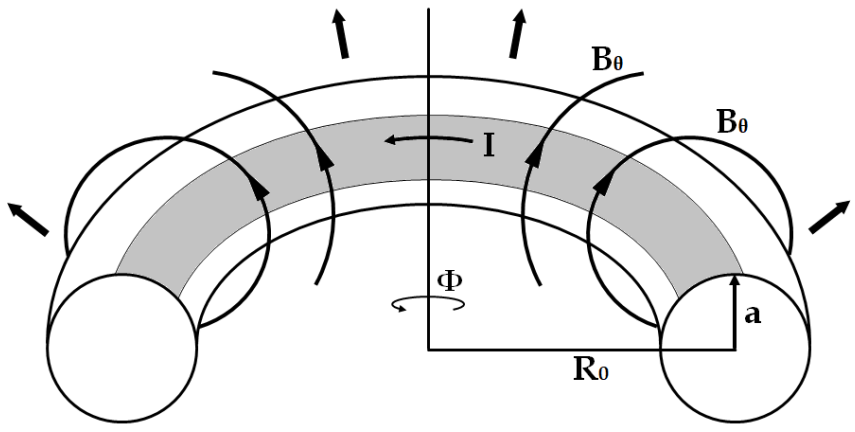

Figure 2.4: A toroidal FR with minor radius a and major radius R_0 with a net current I flowing through it. B_θ is the poloidal field and the arrows pointing outward denotes the hoop force experienced by the FR.

Torok & Kliem, 2006 proposed that a flux rope that expands by this principle will become unstable along the major axis when/if the external poloidal field in the solar atmosphere decays fast enough. They also expanded the conditions for instability that was derived by Bateman

(1978). To understand the mechanisms of the torus instability in a flux rope, a description following that of Priest (2014) is given below.

The torus shown in Figure 2.4, presents a toroidal force-free flux rope with a major radius R_0 and a minor radius a. It has a net current I flowing through it. An outward pointing Lorentz force, so-called hoop force, is associated with this curved current carrying flux rope. Without an external poloidal field such torus cannot be stable. The toroidal current within the flux rope together with the external magnetic field introduces a strapping force in the middle of the torus to nullify the hoop force, resulting will in the equilibrium to the toroidal flux rope. The net force (as given by Priest 2014) is,

$$F = \frac{\mu_0}{4\pi}[\frac{I^2}{R_0}\log_e(\frac{8R_0}{a} - 1) - \frac{Im}{R_0^3}] \tag{2.10}$$

where, the first part of the equation describes the hoop force acting outward, while the second part of the equation describes the strapping force due to the ambient coronal field, which, in this case, is a dipole field with strength m. However, the equilibrium of this torus is dependent on the value of R_0. When $R_0 \rightarrow dR$ there is a loss of equilibrium. dR is the perturbed radius of the torus and when the flux enclosed within the structure F = constant then $R_0 \rightarrow R_0 + dR$. Using this assumption, it is possible to determine the force outside the torus necessary for stability of the torus. However, Bateman (1978) considered the external field to be a constant that was later pointed out to cause reconnection in the rear side of the structure in numerical experiments (Torok & Kliem 2005).

Torok & Kliem (2006) derived the criterion for the stability (or threshold for TI) of the toroidal ring carrying a constant current in an external field by assuming total enclosed flux $F = F_{int} + F_{ext}$. Both the internal (F_{int}) and external (F_{ext}) flux are affected by the change in the major radius of the torus R_0. By assuming a different condition for the external field B_{ext} in the form of $B_{ext} = \hat{B}R_0^{-n}$, they derived the threshold to be $n > 3/2 - 1/(2c) + 1$ where n is the critical decay index for the external field and c is the a flux rope constant given by $c = \log_e(8R_0/a) - 1$. With the establishment of the critical decay index, $n_{crit} = 1.5$, it became clear that a toroidal system will be stable (TI) for values below it (later investigated by: Kliem et al. 2013; Amari et al. 2014). Experiments using toroidal FRs, however, have noted behavior similar to torus instability even when the initial conditions did not exceed the TI threshold (Fan & Gibson 2004, 2007; Fan 2005, 2010). One of the key things discussed later (Chapter 4.4) is the presence of a TI like expansion in the Fan & Gibson FR that is studied in this thesis.

2.4.2 Kink Instability

If a helical perturbation is applied to the FR axis instead of a radial perturbation as in TI, the torus may become helically unstable. This is shown in Figure 2.5 and the related instability is called the helical kink instability. Anzer (1968) concluded that a straight force-free flux rope that extends infinitely long and has some twist tends to exhibit kink-like instabilities. In 1972, Raadu proposed that a line-tied flux rope is more stable. This hypothesis was then confirmed by Hood & Priest (1981) and later by Baty & Heyvaerts (1996). Torok & Kliem (2003) studied the line-tying of a toroidal force-free flux rope with different amounts of twist in order to find a critical value which would act as a threshold for the KI. It was found to be KI when the field lines were wound around the flux rope axis 1.25 times between the line-tied ends.

With the advancements in understanding magnetic helicity and the underlying concepts of twist and writhe of a flux rope, KI has received plenty of attention. Several events have been studied

(e.g., Romano et al. 2003; Williams et al. 2005; Alexander et al. 2006; Cho et al. 2013). A common feature in most studies conducted on the KI is the presence of a twisted flux rope. The KI is set off by the accumulation of magnetic energy in these twisted field lines which are explosively released.

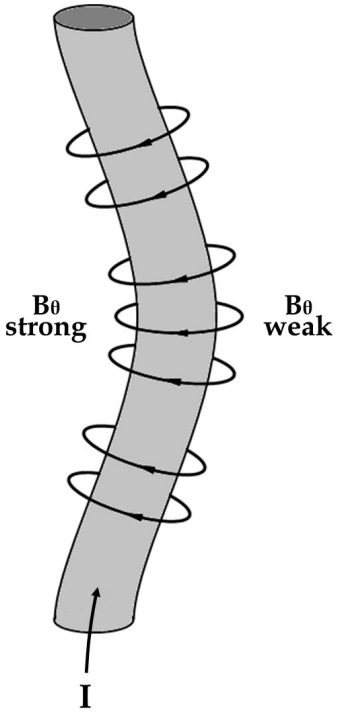

Figure 2.5: A kink unstable flux tube with B_θ, the toroidal magnetic field component and the axial current I due to it. Distortion occurs when B_θ in the concave part is stronger than the B_θ in the convex part

To understand the kink instability, it is necessary to look into the cylindrical MHD equilibrium. For a thorough understanding of the concept, a normal mode analysis is performed to derive the various modes of instability. This analysis can be found in several text books and the description below is limited to the low mode number of the Alfven waves (typically m = 1) with a complex frequency ($\omega^2 < 0$) so that the wave modes keep growing exponentially. These modes are generally called kink modes and are associated with the helical deformations of a plasma structure (Figure 2.6 shows the various kink modes).

A simplification of the dispersion relation for m > 0 gives (Pg. 116, Boyd & Sanderson),

$$\mu_0 \rho \omega^2 = k^2 B_0^2 + [kB_z + \frac{m}{a} B_\theta(a)]^2 - \frac{m}{a^2} B_\theta^2(a) \tag{2.11}$$

where, a is the radius of the cylindrical enclosure that is being considered. Here, the equilibrium magnetic field (B_0) and the toroidal magnetic field (B_z) are constant. B_θ is the poloidal field of the enclosure. Since the kink instability considered here is the m = 1 mode, the above equation can be rewritten with the pressure balance equation as,

$$P_0 + \frac{B_0^2}{2\mu_0} = \frac{B_z^2}{2\mu_0} + \frac{B_\theta^2(a)}{2\mu_0} \tag{2.12}$$

By putting m = 1 in Equation 2.11 and using 2.12 to write it in the form,

$$\omega^2 = \frac{k^2 B_z^2}{\mu_0 \rho}[2 + \frac{2B_\theta(a)}{kaB_z} + \frac{B_\theta(a)}{B_z^2} - \beta_t] \tag{2.13}$$

where β_t is the plasma beta in the corona ($\beta \ll 1$) which suggests that the currents in these twisted cylindrical structures flow in parallel (approximately) to the magnetic field lines. The m = 1 kink mode (Figure 2.5) is only stable for values $|B_\theta/B_z| < |ka|$ where |k| takes integer values which cannot be less than the length of the plasma enclosure (L) since $k = 2\pi/L$. Therefore, the criterion for the stability of a cylindrical tube is given as (Pg. 118, Boyd & Sanderson),

$$|\frac{B_\theta}{B_z}| = \frac{2\pi a}{L} \tag{2.14}$$

The criterion for stability can be given in terms of twist by using Equation 2.14 as,

$$\Phi = \frac{LB_\theta}{aB_z} \tag{2.15}$$

which is the twist of a magnetic field line around the flux rope axis along its length L suggesting that the flux rope can be unstable for any given twist (written in terms of the flux rope radius (a)),

$$\Phi(a) = -Lk \tag{2.16}$$

For coronal plasma, this twist threshold has been identified to be $\Phi(a) = 2.49\pi$ (or 1.25 turns) (Hood & Priest 1981).

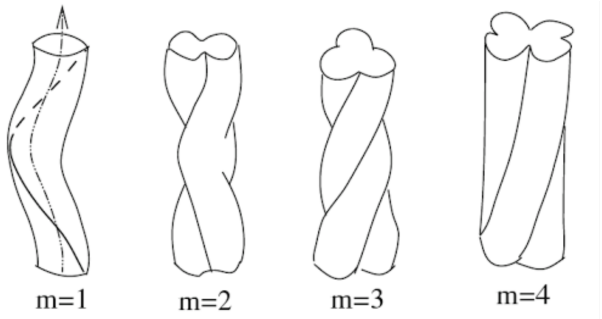

Figure 2.6: The different kink modes (m > 0) (adapted from Cravens 2004)

Figure 2.7 shows a few cases of observed kink unstable FRs in the solar atmosphere. These observed cases (Alexander et al. 2006; Liu & Alexander 2009; Lie et al. 2012; Kliem et al. 2012) involve a twisted flux rope exhibiting writhing and un-writhing due to photospheric shear motions (Isenberg & Forbes 2007). However, for these to be observed, dopplergrams must be available. Questions of whether the kink instability occurs due to eruptions or if it causes them is still debated over. Several models have suggested the presence of TI to be the cause for eruptions (Demoulin & Aulanier 2010). This has particularly been true in case of some numerical studies (Amari et al. 2005; Fan & Gibson 2007; Fan 2010) where an emergence of a flux rope through a time-dependent photospheric boundary is studied. There were signs of these flux ropes exhibiting the TI even when they were not particularly set as the initial conditions for simulations. This is discussed further in Chapter 4 while discussing one of the models (Fan& Gibson 2004) in detail.

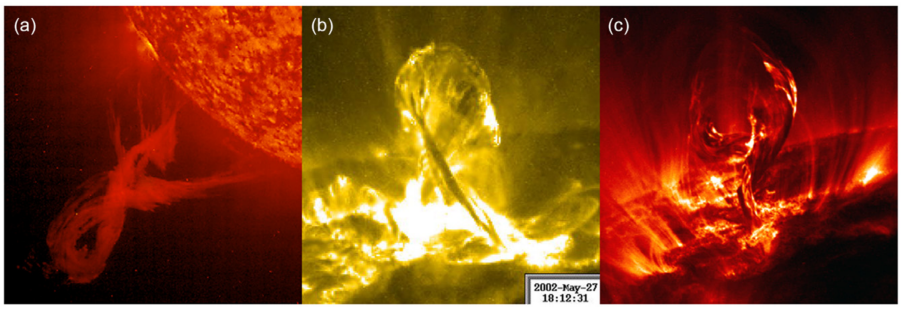

Figure 2.7: Solar filaments exhibiting a kinked structure observed in the extreme ultra violet (EUV) wavelength. (a) The 18 January 2000 eruptive event as observed in 304Åby the EIT telescope on-board the SOHO spacecraft. (b) The 27 May 2002 confined event observed in 195Åby the TRACE satellite. (c) Eruptive event from 19 July 2000 observed in 171Åby TRACE. (courtesy: Torok et al. 2010)

There are several open questions which are yet to be answered concerning the kink instability for the onset of flux rope eruption in the solar atmosphere. Other questions on the likelihood of kink or torus instability to trigger eruptions or the role of reconnection in kink instability also remains a hot topic of discussion. Studies on twist and the conservation of helicity are also under active research (e.g., Lin et al. 2002; Kumar et al. 2012).

Chapter 3

Modeling the solar corona

Distinguishing the coronal magnetic field and its evolution can unlock key information regarding solar eruptions. However, there is a lack of direct measurements available from the corona and the only accurate remote measurements available are locally from the photosphere and from spacecraft observations in the heliosphere. Vector magnetograms provide measurements of the photospheric magnetic field. These magnetograms are necessary for the extrapolation of the coronal magnetic fields.

Advancements in observational technologies have also played a huge role in understanding the coronal phenomena. The corona exhibits high thermal conductivity parallel to the magnetic field which makes the plasma particles visible in certain temperatures. This allows for the observation of these plasma loops which scientists use to find a visual fit of the magnetic field lines using computer models.

To study the coronal fields and to understand eruptive structures, it is imperative to discuss the role of theoretical models. As with any model, it is important to make a few assumptions, starting with the assumption of the corona being in a potential state (current-free). This assumption, while not completely applicable to the entire corona, can still be used to study most regions. A brief overview of this assumption is provided at the end of Chapter 1.3.3. Equation 1.6 gives the minimum energy of a system (ground state) called the potential field. Applying this to coronal models requires an accurate measurement of the photospheric magnetic field (which is available) (Schrijver et al. 1997). The magnetic field lines that reach the outer boundary (source surface) are forced to be radially outward.

Figure 3.1 shows a potential field source surface (PFSS) model produced by the NASA's Goddard Space Flight Center Scientific Visualization Studio. The model is a rough evolution of the coronal magnetic field between the years 1997 and 2013. It can be noted that the magnetic field lines are either closed or extend radially as solar wind. The model, being only a rough estimate, does not consider the dynamics of the solar corona which lead to energetic events such as CME. This brings the need for other theoretical models such as the magnetohydrodynamic (MHD) model which is discussed in the later sections of this chapter.

3.1 Force-free fields

Most of the corona and the chromosphere are dominated by the magnetic pressure (low beta ($\beta \ll 1$)). A balance between the pressure gradient, gravitational force and the Lorentz force

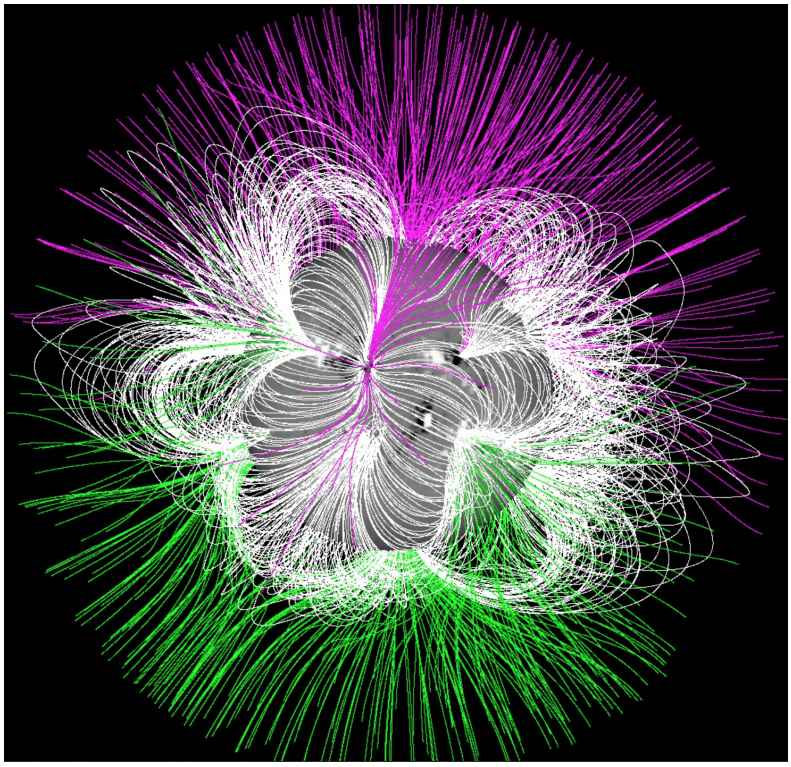

Figure 3.1: Potential field source surface(PFSS) model where the closed field lines are colored white while the open field lines in the northern and southern hemisphere are colored pink and green respectively. (credits: NASA's Goddard Space Flight Center Scientific Visualization Studio)

is necessary to attain equilibrium. The hydrostatic pressure balance equation can be used to study the distribution of plasma along the coronal magnetic field lines,

$$0 = -\nabla P + \mathbf{J} \times \mathbf{B} + \rho \mathbf{g} \tag{3.1}$$

In the regions considered, the magnetic forces dominate. Equation 3.1 becomes,

$$\mathbf{J} \times \mathbf{B} = 0 \tag{3.2}$$

However, unlike with the potential state when the system is current-free ($\mathbf{J} = 0$), here, $\mathbf{J} \neq 0$. This would mean that the magnetic field and the current are parallel to each other,

$$\nabla \times \mathbf{B} = \mu_0 \mathbf{J} \tag{3.3}$$

$$\mu_0 \mathbf{J} = \alpha \mathbf{B} \tag{3.4}$$

where α is the force-free parameter and it is a scalar function of position. By combining equation 3.3 and 3.4,

$$\nabla \times \mathbf{B} = \alpha \mathbf{B} \tag{3.5}$$

Here, $\mathbf{B}$ must satisfy,

$$\nabla \cdot \mathbf{B} = 0 \tag{3.6}$$

By using equation 3.6 in equation 3.5,

$$0 = \nabla \cdot (\nabla \times \mathbf{B}) = \nabla \cdot (\alpha \mathbf{B}) = \mathbf{B} \cdot \nabla \alpha \tag{3.7}$$

$$\mathbf{B} \cdot \nabla \alpha = 0 \tag{3.8}$$

This relation shows that α is a constant along a magnetic field line although, it may be different for each individual field line. An assumption that the force-free parameter $\alpha = 0$ would make the system potential. Assuming a constant α in equation 3.5 gives,

$$\Rightarrow \nabla \times (\nabla \times \mathbf{B}) = \nabla \times (\alpha \mathbf{B}) = \alpha \nabla \times \mathbf{B} = \alpha^2 \mathbf{B} \tag{3.9}$$

$$\nabla \times (\nabla \times \mathbf{B}) = \nabla(\nabla \cdot \mathbf{B}) - \nabla^2 \mathbf{B} \tag{3.10}$$

Combining equation 3.9 and 3.10 gives the vector Helmholtz equation:

$$-\nabla^2 \mathbf{B} = \alpha^2 \mathbf{B} \tag{3.11}$$

The solutions to the Helmholtz equation are used in numerical models (Chiu & Hilton 1977; Alissandrakis 1981) and are called Linear force-free models (LFFF).

By assuming a non-constant α which would now behave as a scalar function of position,

$$\nabla \times (\nabla \times \mathbf{B}) = \nabla \times (\alpha \mathbf{B}) \tag{3.12}$$

a non-linear equation can be arrived at,

$$\nabla^2 \mathbf{B} + \alpha^2 \mathbf{B} = \mathbf{B} \times \nabla \alpha \tag{3.13}$$

Solutions to equation 3.13 along with the equation 3.8 are used in numerical models and are called Non-linear force free models (Neukirch 2005; Schrijver et al. 2006, 2008; Wiegelmann et al. 2012).

3.2 Magnetohydrodynamics (MHD)

The Plasma is a many body system with a large number of ions and electrons. To get a macroscopic description of the plasma as a system, it is necessary to make assumptions. One such assumption is based on the consideration of plasma as a single conducting fluid which expresses mass, momentum and energy conservation along with electrodynamics. This single fluid description is called Magnetohydrodynamics (MHD). It is widely regarded as the most simple and self consistent description of plasma dynamics and is used in describing solar and other astrophysical phenomena.

Since the solar coronal magnetic fields are generally too weak to be measured using Zeeman measurements, they are extrapolated from the photospheric magnetic fields and are then compared with the geometries noticed observationally. These computer models are of several kinds with a few of them discussed in the previous section. However, none of those models consider the plasma dynamics or its time scales like MHD does. In MHD, a plasma is a fluid with velocity $\mathbf{V}$, pressure P and density ρ under the influence of a magnetic field $\mathbf{B}$.

The equations governing the plasma are the equations of fluid dynamics and Maxwells equations. Starting with Maxwell's equations,

$$\nabla \cdot \mathbf{B} = 0 \tag{3.14}$$

MHD assumes that the plasma is non-relativistic in the corona and therefore, Ampere's law can be written as,

$$\nabla \times \mathbf{B} = \mu_0 \mathbf{J} \tag{3.15}$$

where $\mathbf{J}$ is the current density. Faraday's law in the set of electrodynamic equations governing the plasma in MHD is given as,

$$\nabla \times \mathbf{E} = -\frac{\partial \mathbf{B}}{\partial t} \tag{3.16}$$

To close the system of equations 3.14, 3.15 and 3.16, Ohm's law is used,

$$\mathbf{J} = \sigma(\mathbf{E} + \mathbf{V} \times \mathbf{B}) \tag{3.17}$$

The electric conductivity, $\sigma \to \infty$ for perfect conductivity. Combining the above equation (3.14, 3.15, 3.16, 3.17) would eliminate the electric field $\mathbf{E}$ in the induction equation,

$$\frac{\partial \mathbf{B}}{\partial t} = \nabla \times (\mathbf{V} \times \mathbf{B}) + \eta \nabla^2 \mathbf{B} \tag{3.18}$$

$\eta = 1/\mu_0 \sigma$ is the magnetic diffusivity. The equation can be divided into two parts; the first part describes convection while the second part describes diffusion.

As mentioned earlier, the MHD fluid equations describe its mass, momentum, and energy conservation. The mass continuity equation is given as,

$$\frac{\partial \rho}{\partial t} = -\nabla \cdot (\rho \mathbf{V}) \tag{3.19}$$

Both plasma velocity $\mathbf{V}$ and magnetic field $\mathbf{B}$ are coupled through the Lorentz force ($\mathbf{J} \times \mathbf{B}$) and the Ohm's law (Equation 3.17) in the momentum equation, which is given by,

$$\rho \frac{D\mathbf{V}}{Dt} = -\nabla P + \mathbf{J} \times \mathbf{B} + \rho \mathbf{g} \tag{3.20}$$

Since in most of the corona the magnetic forces are stronger than all the other forces, the pressure P and gravity $\mathbf{g}$ can be neglected. And finally, if the plasma does not experience any heating or conduction, the system is adiabatic,

$$PV^{\gamma} = \text{constant}. \tag{3.21}$$

γ is the ratio of specific heats. The above MHD description is a simplified form and can be applied to most of the solar corona.

3.3 Dynamic modeling of the coronal magnetic field

There has been a number of models in the past few decades which have tried to understand the solar atmospheric structures and their evolutionary dynamics that lead to eruption (Amari et al. 2003a,2003b; Fan 2010; Aulanier et al. 2010; Kusano et al. 2012; Amari et al. 2014, Inoue et al. 2015). Basic details on some models are briefly discussed in the previous sections of this chapter. These theoretical models are studied numerically through simulations which recreate the above mentioned coronal structures and dynamics to better complement observational data.

A good starting point would be with the PFSS model, one of the simplest models for for computing the coronal magnetic field. It offers a quick overview of the field structure which can then be used as a reference to study a particular local region with one of the force-free models (Wiegelmann & Neukirch 2002). However, the force-free reconstructions are just snapshots and are not used in studying the dynamic features of the magnetic field such as its evolution. Studying the dynamic evolution can help understand the onset of eruption and the instabilities (Torok & Kliem 2005, 2006) that may occur. In order to capture the details, it is necessary to simulate the coronal fields using an MHD model with boundary conditions from other force-free extrapolations (Amari et al. 2003; Wu et al. 2005). By numerically solving the set of MHD equations in time, it should be possible to evolve the coronal fields to produce eruptive events (Jiang et al. 2012, 2014, 2016).

3.3.1 Modeling with MHD

Modeling with MHD provides a significant improvement over static models (Section 3.1). If the goal is the investigation of different dynamic processes in the solar atmosphere, the model must include a description of plasma in these regions as well. MHD provides a simple and efficient description of the plasma which is self-consistent based on the approximations. This allows for simulations of plasma and magnetic field interactions well beyond the solar atmosphere (Riley et al. 2011; Feng et al. 2012).

The goal of modeling is to simulate the coronal magnetic field and its structural evolution in a realistic way. Development in modeling techniques during the past decade has produced "realistic" models (Riley et al. 2006; Lionello et al. 2009; Feng et al. 2012; Jiang et al. 2016). Further details about these models can be found in the review by Mackay et al. (2012). A variety of existing MHD models have been constructed based on what they are applied to investigate. Such a diverse availability is a main reason to why MHD is used in modeling solar phenomena. Fan & Gibson (2004), whose model is used for the work in this thesis, use a simplified form of MHD to study the ideal kink instability (Torok & Kliem 2005, 2006).

Recent development in computational technologies has allowed for more realistic global MHD models (albeit non-eruptive) (Lionello et al. 2005; Riley et al. 2011). These models use a time-dependent photospheric boundary condition which evolve the coronal magnetic fields with changing photospheric conditions. Applications of these models can be found in reviews by

Forbes et al. (2006) and Chen (2012). Vazquez et al. (2008) compared two global models (Hayashi 2005; Cohen et al. 2007) with observations and found them to be closely agreeing for most parts except for the polar regions which had different densities.

Although they having various applications in solar physics, MHD models have their drawbacks. One major drawback and a reason for the work in this thesis is the computational requirements for solving the full 3D MHD equations. Even though MHD is widely regarded as a successful model, it is still a heavy approximation of the plasma which is a many body system. Some features of eruption such as shockwaves and reconnection can be investigated further when moving away from the single fluid description. A kinetic description analyzes the distribution functions and would be very useful in investigating the motions of plasma particles in the heliosphere. However, current goals in the computational field are to improve existing MHD models to be more efficient. Meanwhile, there have been new models which have been developed to find a compromise between studying complex dynamics and their computational requirements. One such model is the magneto-frictional method (MFM) (Yang et al. 1986).

3.3.2 Magneto-Frictional Method

Yang et al. (1986) developed a method closely related to the variation of MHD known as the MHF(Magneto-hydrofriction) method suggested by Chodura & Schluter (1981). This method, which they termed "Magneto-Friction" or the MF-method (or simply MFM) assumes a magnetic field which is frozen into a "highly conducting medium" in space that the plasma in this system experiences a frictional force when it moves. The MHD equation of motion changes to,

$$\rho\frac{\mathrm{D}\mathbf{V}}{\mathrm{D}t} = -\nabla \mathrm{p} + \mathbf{J}\times\mathbf{B} + \rho\mathbf{g} - \nu\mathbf{V} \tag{3.22}$$

where ν is a frictional coefficient. In case of a low-β environment (such as the low corona), the corona is force-free for most cases and the above equation can therefore be simplified as,

$$\rho\frac{\mathrm{D}\mathbf{V}}{\mathrm{D}t} = \mathbf{J}\times\mathbf{B} - \nu\mathbf{V} \tag{3.23}$$

van Ballegooijen et al. (2000) developed this method further by ignoring the inertia term ($\mathrm{D}\mathbf{V}/\mathrm{D}t = 0$) in equation 3.23,

$$\mathbf{V} = \frac{\mathbf{J}\times\mathbf{B}}{\nu} \tag{3.24}$$

This suggests that the velocity in the MF relaxation can be obtained directly from the magnetic field $\mathbf{B}$. By using this velocity in the induction equation (Equation 3.18),

$$\frac{\partial\mathbf{B}}{\partial t} = \nabla\times(\mathbf{V}\times\mathbf{B}) - \eta\nabla^2\mathbf{B} \tag{3.25}$$

η, the diffusion coefficient is non-zero. The diffusivity η allows the change in magnetic topologies suggesting magnetic reconnection. These changes can be modeled, but the heating that appear alongside the reconnection is not modeled. Equation 3.25 can be used to drive the evolution of the magnetic field. Yang et al. (1984) suggested that the total energy ($\mathrm{W} = \int \mathrm{B}^2/(2\mu_0)\mathrm{d}^3\mathrm{x}$)decreases monotonically until it reaches a force-free state $\mathbf{J}\times\mathbf{B} = 0$. When the conductivity is finite, the energy dissipates until a force-free state is reached. This has allowed

the MFM to be used to compute NLFFF with proper photospheric boundary conditions (Valori et al. 2005; Valori et al. 2007).

Mackay & van Ballegooijen (2006) developed this further and provided a dynamic boundary condition which would allow the MFM to be time-dependent unlike the MF-NLFFF schemes. This time-dependent MFM has been utilized to some success in modeling the coronal magnetic fields (Mackay & van Ballegooijen 2006a, 2006b; Chueng & DeRosa 2012).

The MFM, while being a realistic alternative to MHD, has disadvantages. While the MFM is computationally affordable compared to MHD, it does not capture the plasma dynamics such as heating and acceleration of plasma particles. Due to the ad hoc nature of the frictional coefficient ν and the frictional velocity $\mathbf{V}$, the time evolution captured using MFM may not be real. However, with a good choice of the MFM parameters, it has been quite accurate in modeling the dynamic coronal phenomena. The issues with choosing the right magneto-frictional coefficient is partly addressed by Valori et al. (2007) who suggested that $\nu \sim B^2$ since it relaxes magnetically weak regions.

Pagano et al. (2013) proposed evolving the coronal field in MFM and using it as an initial condition for MHD. This would eliminate part of the computation and time requirements in solving for full-MHD solutions. Current issues in the further development of the MFM is to find realistic photospheric boundary conditions. Estimating the photospheric electric fields accurately is a difficult task due to the. A very detailed analysis of the techniques that can be used to find the photospheric $\mathbf{E}$ are provided by Kazachenko et al. (2015).

Chapter 4

Numerical Simulations of the ideal MHD kink instability using the Magnetofrictional Method

Several models have been proposed for describing the evolution of the coronal magnetic field during solar eruptive phenomena. However, studying dynamic evolution on long time scales by employing an MHD model is challenging and computationally very expensive. Among may others, Fan & Gibson (2004) used MHD to study the "kinematic flux emergence" into an initially potential magnetic field arcade. In contrast, the magneto-frictional model has been successfully applied for long time scales at a relatively low cost. As a fairly new method, a time-dependent MFM has not yet been utilized in studying ideal MHD phenomena such as instabilities. The work in this thesis is aims at employing a time-dependent MFM to recreate the work of Fan & Gibson (2004). The objectives for this were set in accordance with the aim and are as follows:

1. Exploring the capabilities of the MFM in capturing the (slow) energization of the coronal magnetic field.
2. Investigating the model for different values of the magneto-frictional coefficient ν.
3. Reproducing an ideal MHD instability using MFM.
4. Comparing the changes in the flux rope with different values of twist and their height above the bottom boundary $z = 0$
5. Addressing the presence of a sigmoidal current sheet during the onset of kink instability.

In order to achieve the above objectives, a tool developed by the space science group in the University of Helsinki was used. It is worthwhile to perform simulations of coronal dynamics in idealized settings. Such experiments can be conducted in a well controlled way, in which, effects such as numerical instabilities, grid resolution issues, etc., can robustly be taken into account.

4.1 The Fan & Gibson model

Fan & Gibson (2004) presented a detailed study of the "kinematic emergence" of a twisted flux rope into a three dimensional coronal magnetic field arcade. In their simulations, the emergence of flux is provided as a dynamic photospheric boundary condition. The coronal magnetic field

is line tied to the photospheric surface and changed with the emergence of the flux rope. The FR may be kink unstable depending on how twisted it is. The technical details of the model study is described in this section.

4.1.1 The FR setup

It is essential to understand the flux rope model before investigating its dynamic evolution in an evolving magnetic field configuration. The Fan & Gibson (FG here onwards) FR has a toroidal geometry and is given in polar coordinates (r, θ, ϕ),

$$\mathbf{B}_{\text{tube}} = \nabla \times [\frac{\mathbf{A}(r,\theta)}{r\sin\theta}\hat{\boldsymbol{\phi}}] + B_{\phi}(r,\theta)\hat{\boldsymbol{\phi}} \tag{4.1}$$

where, $\mathbf{A}$ is the vector potential and is given by,

$$\mathbf{A}(r,\theta) = \frac{1}{2}qa^2B_t exp[-\frac{\varpi^2(r,\theta)}{a^2}] \tag{4.2}$$

B_{ϕ} is the toroidal component of the magnetic field,

$$B_{\phi}(r,\theta) = \frac{aB_t}{r\sin\theta}exp[-\frac{\varpi^2(r,\theta)}{a^2}] \tag{4.3}$$

ϖ in the above equation is the distance to the flux rope axis. The expression is later discussed in Section 4.4.1.

$$\varpi = (r^2 + R^2 - 2rR\sin^2\theta)^{\frac{1}{2}} \tag{4.4}$$

In the above set of equations, B_t is the magnetic field strength along the toroidal tube axis, r, θ, and $\hat{\phi}$ are the radial distance, polar angle and the azimuthal unit vector. The parameter q is the number of of field line twists around the axis and is given in rad a^{-1}. It can take positive or negative values depending on the direction the magnetic fields need to be twisted. Finally, a is the radius of the tube while R is distance between the origin of the FR and the axis of the FR.

Figure 4.1 shows only half of the FR placed below the simulation domain. For half the torus, the average number of field line rotations is half of the full FR. The field lines wind more tightly towards the axis compared to the outer flux surface.

4.1.2 The Simulation set up

The FG2004 model assumes the coronal magnetic field to be line tied to the photospheric boundary with an initial force-free condition which changes in time with changing photospheric boundary conditions.

Their simulation considers a 3D Cartesian domain as seen in Figure 4.1. The initial pre-existing potential arcade field and the FR placed below the bottom boundary can be seen in Figure 4.1. The distribution of the magnetic field at the photospheric boundary ($z = 0$) is given by,

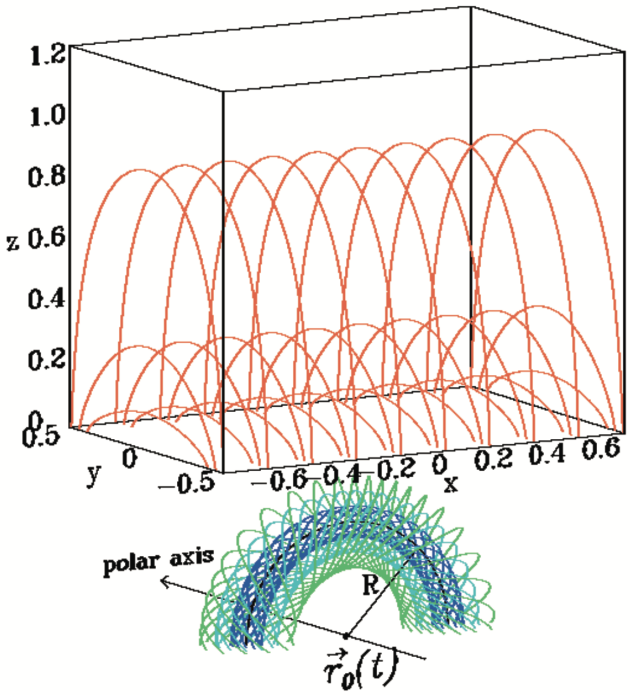

Figure 4.1: Setup of the FG2004 experiment using MHD. The pre-existing potential field arcade is represented by the set of arched field lines in red. The FR with its origin $\mathbf{r}_0(t)$ in its initial position below the photospheric boundary (image adapted from Fan & Gibson 2004)

$$B_{z|z=0} = \begin{cases} B_0, & y < y_+, \\ B_0 \exp[-\frac{(y-y_+)^4}{w^4}], & y_+ < y < y_+ + 2w, \\ 0, & y_+ + 2w < y < y_- - 2w, \\ -B_0 \exp[-\frac{(y-y_-)^4}{w^4}], & y_- - 2w < y < y_-, \\ -B_0, & y_- < y, \end{cases} \tag{4.5}$$

Here, $y_+ = -0.4L$, $y_- = 0.4L$ and $w = 0.05L$ (Here, L is the size scale of the domain and is chosen to be $\approx 0.1R_\odot$. This is the pressure scale height H_p of the 2MK corona). The above set of equations were used to set up the initial potential field configuration. As discussed in a previous chapter (3.1), in an initially potential configuration, the corona is current-free and becomes energized with the introduction of a current carrying structure. However, this alone does not lead the flux rope to the onset of eruption. For a flux rope which emerges as a monolithic structure to exhibit eruptive behavior, certain ingredients are necessary. In FG2004, this happens when the FR reaches a certain point in the emergence (see Section 4.4) when it becomes kink unstable. It depends primarily on the twist that is transported into the corona (given by the q parameter).

The FG model emphasizes the relation between the poloidal field component of the emerging flux rope and the direction of the preexisting coronal magnetic field arcade. Both are configured in a way that they are in the same direction to avoid creating a magnetic field gradient which when high leads to reconnection between the field lines. This way, the FR emerges quasi-statically without reconnection until the onset of kink instability.

The boundary driving of the emerging FR ($\mathbf{B}_{\text{tube}}$) into the photosphere is due to a time-dependent electric field ($-\mathbf{V} \times \mathbf{B} = \mathbf{E}$) with a constant speed $V_0\hat{z}$,

$$\mathbf{E}|_{z=0} = -V_0\hat{z} \times \mathbf{B}_{tube}(x, y, z = 0, t) \tag{4.6}$$

Figure 4.1 shows the FR below the photospheric boundary. The origin of the FR ($r_0(t) = (-0.675L + V_0(t)\hat{z})$ is allowed to rise at a constant speed. The velocity $\mathbf{V} = 0$ across the lower boundary except for the region of flux emergence where the boundary velocity $\mathbf{V} = V_0\hat{z}$.

MHD simulations

The simulations are performed in a three dimensional Cartesian domain with dimensions; $x = [-0.75L, 0.75L], y = [-0.5L, 0.5L], z = [0, 1.25L]$. L is the size scale of the domain and is chosen to be $\approx 0.1R_{\odot}$. This is the pressure scale height H_p of the 2MK corona.

For the MHD simulations, FG2004 considered the toroidal magnetic field strength to be $B_t = 9B_0$, where $B_0 = 0.1T$. The number of field line twists was $q = -1.25$ rad a^{-1} (left handed twist), and the minor radius of the FR was set to, $a = 0.1L$. These values were left unchanged throughout all runs in the simulation.

In their first run, the FR emerged into the simulation domain and was stopped when the origin of the FR (r_0) reached $z = 0$. The FR became kink unstable and a thin sigmoidal current sheet was formed around the foot points which are connected along the polarity inversion line (Figure 4.2). They performed another run where they stopped the FR prematurely at 0.250L with. The FR failed to become kink unstable since it had not reached the critical twist needed for the onset of instability. The results of this were used to study the FR behavior when it reached the critical twist needed for a line tied FR to be kink unstable. They also investigated the current sheet that was formed at the onset of instability. A third run was made with better spatial resolution to run the first simulation again. The motive behind this was to have a better resolved current sheet. The results of this experiment were discussed in detail in their publication from 2004 (Fan & Gibson 2004). The results from FG2004 are used as a reference for simulations using MFM. This is to compare if MFM as a model is capable of reproducing MHD phenomena.

There is some important information to keep in mind while investigating this model. Firstly, Flux emergence is a complicated phenomena and there are questions of whether an FR can emerge as a whole given the weight of the plasma it carries is still debated (Fan 2001; Archontis et al. 2004, 2009). However, several recent models have been able to achieve an eruption in a non-kinematic setting (emergence in a stratified medium) (MacTaggart & Hood 2009; Archontis & Hood 2012). Secondly, the direction of the coronal magnetic field and the poloidal component of the emerging FR have to be the same. If their directions do not match, excessive reconnections occur between the FR and the overlying arcade from the point of emergence and thus results in a destroyed FR.

4.2 Fan & Gibson model using MFM

The Fan & Gibson model discussed in Section 4.1 is used as a guide for the MFM study in this thesis. The model describes the emergence of a flux rope into a pre-existing coronal arcade which energizes the initial potential arcade field and subsequently erupts (induced by the kink instability) or fails to erupt depending on the properties of the overlying magnetic field and the emergence.

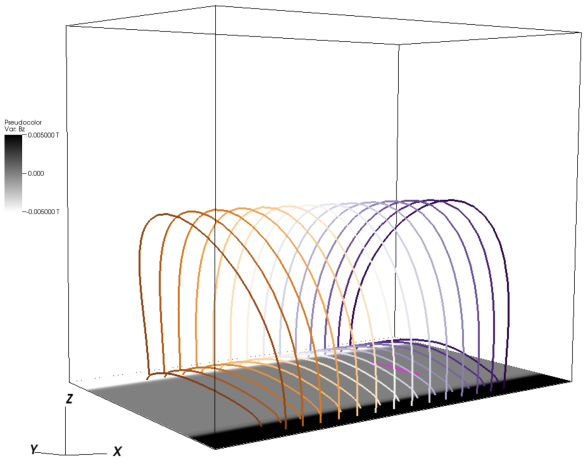

Figure 4.2: Setup of the pre-existing potential field arcade tied to the photospheric boundary. The gray scale plane shows the normal component of the magnetic field at the lower boundary (black = away from the Sun).

The goal of this thesis is to recreate the dynamics of the flux rope emerging into the preexisting arcade detailed earlier using the magneto-frictional method. The MFM assumes that the magnetic fields tend to relax towards a force-free state by introducing an artificial frictional term. This leads to plasma properties being ignored by the model. In order to study dynamic evolution, the topological signatures of the magnetic fields are investigated.

4.2.1 Setting up the experiment

The setup of the FR and the pre-existing potential arcade are similar to the set-up discussed in Section 4.1. Similar to the pre-existing coronal field arcade set up by FG, they are tied to the photospheric boundary. The MFM assumes line tying of the coronal magnetic field arcade all over the photospheric surface. Figure 4.2 shows the resultant coronal arcade. The colored field lines denote field lines originating from a particular point on the surface.

The magnetic field B_z points outward radially from the photosphere. It is is given by Equation 4.5 where; $y_+ = -0.4L$, $y_- = 0.4L$ and $w = 0.05L$. After the initial arcade field is set up, it is changed with time as the boundary conditions at the photosphere change through the electric field **E** given by Equation 4.6. Unlike in FG2004, MFM does not have a characteristic Alfven speed. The speed of emergence is a free parameter and can be chosen by the modeler. For this study, the speed $\mathbf{V}_m\hat{z}$ (the subscript m denotes the boundary driving speed in the MFM simulations) is chosen to be 25 km/s at $z = 0$ (photospheric boundary).

$$\mathbf{E}|_{z=0} = -V_m\hat{z} \times \mathbf{B}_{tube}(x, y, z = 0, t) \tag{4.7}$$

$\mathbf{B}_{tube}$ is the emerging FR and it is represented in a local spherical system and can be found in Equation 4.1. As illustrated in Figure 4.1, the polar axis of the flux tube is parallel to the y-direction of the domain. The primary flux rope constants are kept identical (Section 4.1.2) to FG2004 in order to produce comparable results for analysis.

4.2.2 Magneto-frictional coefficient (ν)

The frictional coefficient is discussed briefly in Chapter 3.3.2. In numerical experiments, the frictional coefficient is chosen by the modeler. In equation 3.24, ν is an ad-hoc parameter which is chosen according to convenience. By testing different values for the frictional coefficient, the following observation is made: Depending on the boundary driving speed ($V_m\hat{z}$ in Equation 4.7), the frictional term is chosen so that the magnetic field arcade evolves in accordance to the flux emergence. This evaluation is done to avoid a mismatch between the boundary driving speed and the boundary conditions which can lead to unphysical phenomena at the bottom boundary. For example: High values for the frictional coefficient can effectively destroy the flux rope by not letting it emerge.

The value for the frictional coefficient was hence chosen to be $\nu = 10^{-13}\mathrm{s/m}^2$. A more analysis of the frictional coefficient can be found in Cheung & DeRosa (2012).

4.3 MFM Simulations

The simulations are divided into four primary scenarios. The first three involve changing the FR twist and for the last scenario, the FR is truncated at different heights (FR height above the photospheric surface). The scenarios are then analyzed for different behavioral dynamics of the FR in the low corona. How well the MFM was able to capture this is discussed by comparing it to the MHD simulations by FG2004.

4.3.1 Evolution of the Coronal field arcade

One of the objectives for the simulation work was to study the evolution of the coronal field arcade over time. The work presented here uses the MFM (brief description in Section 3.3.2) to study the evolution of the coronal arcade with the emergence of a twisted FR.

Figure 4.2 shows a snapshot of the three-dimensional coronal magnetic field arcade. The movie clip (label: FRemergence3D.mp4) presented as part of this e-thesis shows the dynamic evolution of the coronal arcade and the kinking of the twisted FR from two perspectives. The field lines which represent the FR in these snapshots are those wound about its axis. The directions of the magnetic field lines in the arcade are in the same direction as the poloidal component of the FR magnetic field. The snapshots also show that the emerging FR changes the topologies of the initially potential arcade field. Due to the current-free state of the initial coronal magnetic field, the slow transportation of a current carrying flux rope energizes the coronal fields. With time and with the necessary ingredients (twist, height), the FR becomes unstable and exhibits kink instability.

4.3.2 Studying the onset of kink instability

The different scenarios studied here are based on varying the twist and the height at which the FR is stopped. The behavior of the FR changes in each of these scenarios. A fully emerged FR has a different effect on the overlying fields compared to an FR which is stopped. Depending on the amount of twist and stop height, the writhing can also change. The FRs also experiences

an upward acceleration and expansion on their leading edge. The scenarios below are labeled after the number of field line twists q.

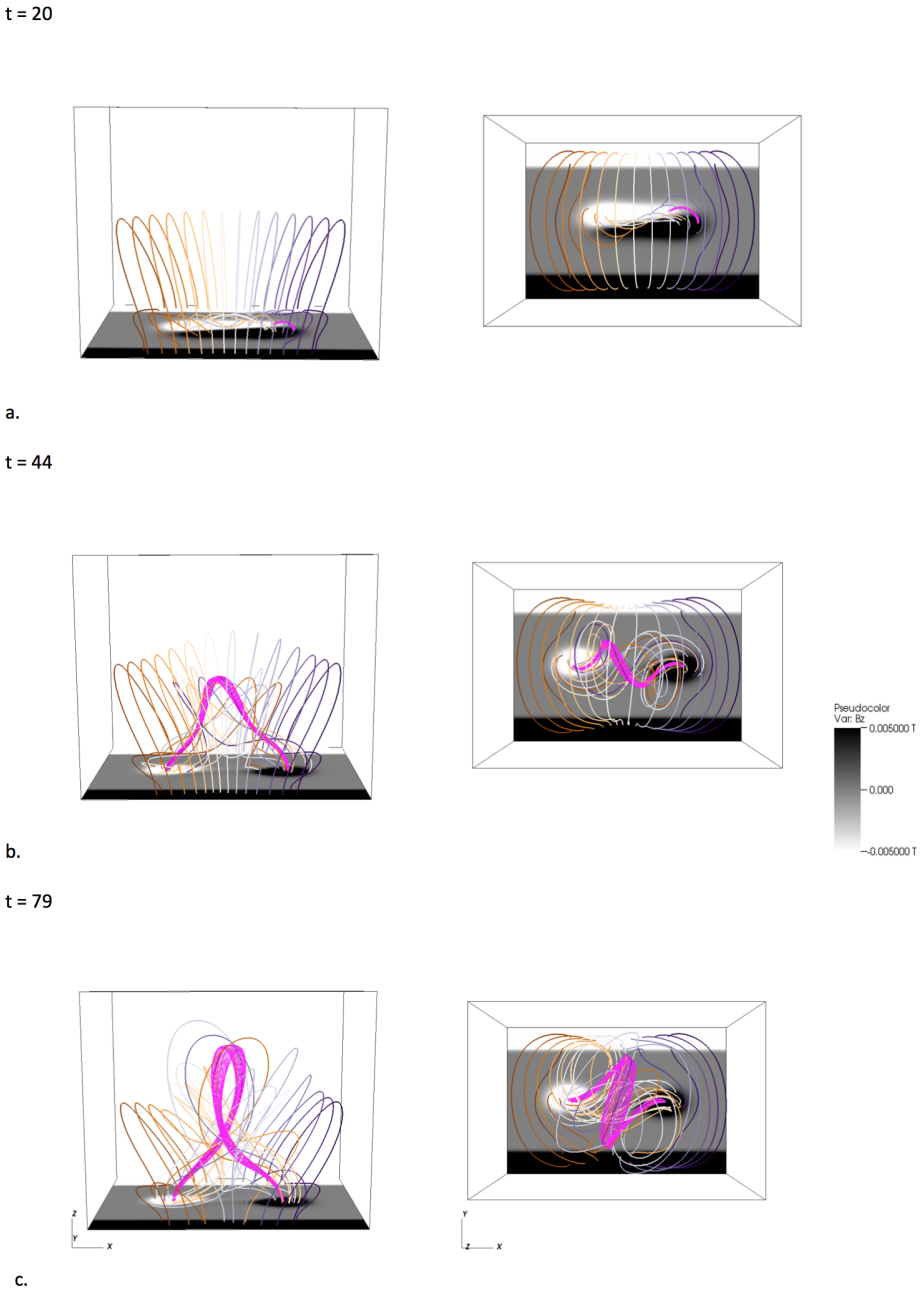

Figure 4.3: Snapshots as viewed from the side (*left* panels) and the top (*right* panels) of the evolution of the three-dimensional coronal magnetic field. The emerging FR has a field line twist of q = -1.25 rad a^{-1} and is stopped when the origin r_0 of the torus is at z = 0.

q = -1.25 rad a^{-1} scenario

In this scenario, the values for the different parameters used in the study are kept mostly identical to that of FG2004. The FR is allowed to emerge at a speed V_m = 25 km/s. The frictional coefficient for this simulation run is $\nu = 10^{-13} sm^{-2}$ (Section 4.2.2) . The number of field line twist of the emerging flux rope is kept the same as FG2004 at q = –1.25 rad a^{-1} turns (negative sign denotes left handed twist). The boundary driving is halted when the origin of

the FR (r_0) reached z = 0. This configuration of twist and height was highly kink unstable in FG2004.

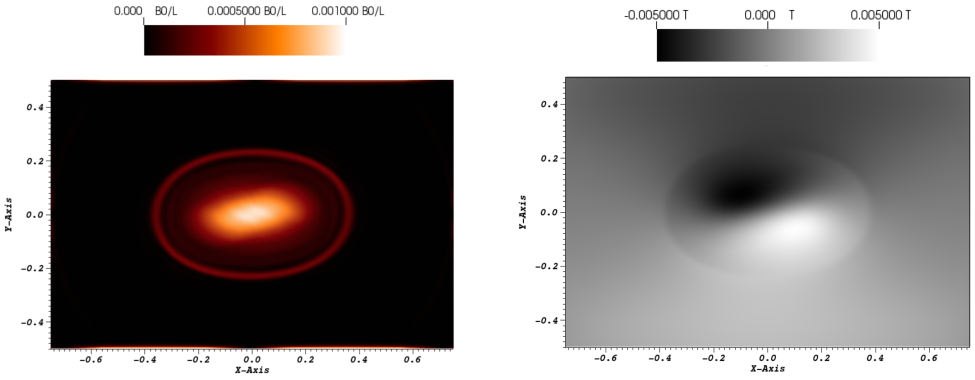

Figure 4.4: Plots showing the horizontal cross sections of the current density |**J**| (*left*) and the magnetic field B_z (*right*) at z = 0.25 at t = 36.

Figure 4.3 shows snapshots of the time evolution of the coronal magnetic field in response to the emerging FR. As seen from Figure 4.3b and 4.3c, between the time from the two snapshots were taken, the FR axis expands upward and writhes. This scenario considers the FR to have the critical twist necessary ($q = -1.25\,\mathrm{rad\,a^{-1}}$) for an FR to be kink unstable. The emergence is stopped at t = 44 (close to Figure 4.3b) and the leading edge of the FR expands and leads to the onset of kink (Figure 4.3c). This expansion at the top of the FR is due to the FG flux rope being inherently torus unstable. This is later discussed in Section 4.4. Figure 4.4 shows a plot of current density |**J**| during flux emergence at t = 36 and the density of the current plotted there is from the top of the twisted flux rope. A very feint current is seen at the borders of the FR where it is in contact with the overlying arcade. This changes as the FR continues to emerge and is seen in Figure 4.5 where the current density at t = 79 appears in the form of a sigmoid suggesting the onset of kink instability. This is very similar to the result produced by FG2004 for the same configuration.

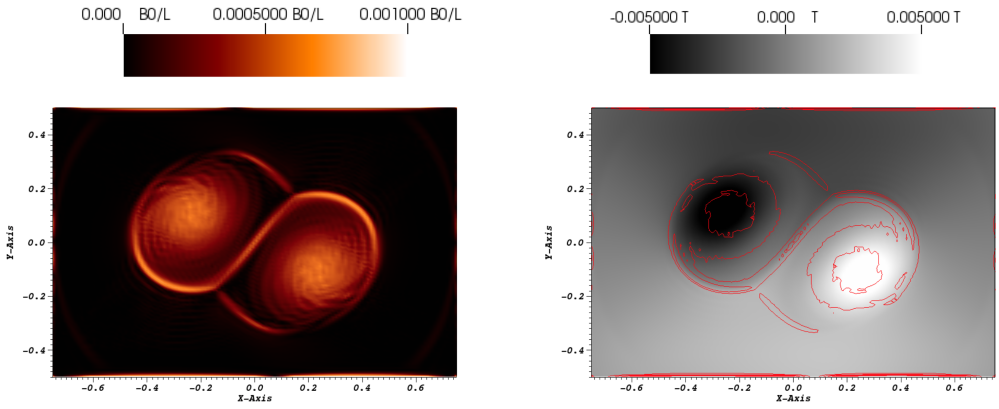

Figure 4.5: Plots showing the horizontal cross sections of the current density |**J**| (*left*) and the magnetic field B_z (*right*) at z = 0.25 during the onset of kink instability of an FR with twist q = - 1.25 $\mathrm{rad\,a^{-1}}$ turns. A contour of the current density |**J**| is superimposed with the magnetic field B_z for reference.

One of the key motivations behind studying the FG2004 simulations was to see if the MFM was able to reproduce an ideal MHD instability with the necessary dynamics in the coronal magnetic field. As shown here, the MFM is capable of producing kink unstable FRs. This result is discussed in detail in Section 4.4.

Low twist ($q = -0.75$ rad a^{-1}) **scenario**

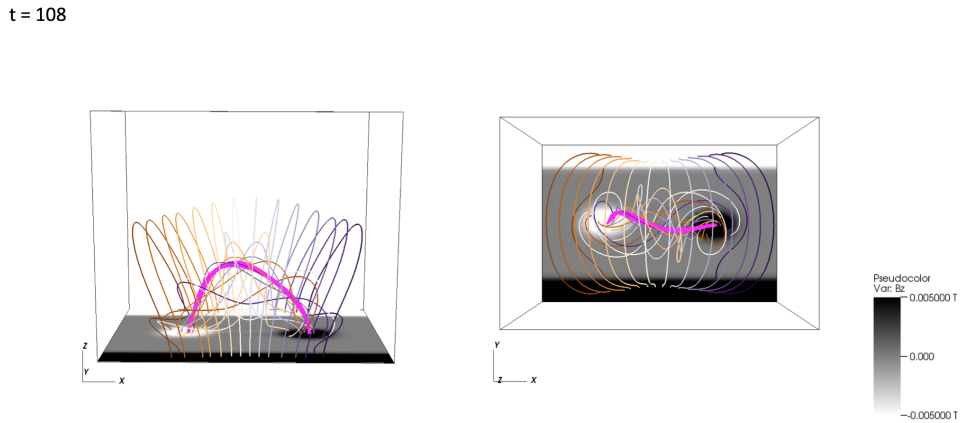

Figure 4.6: Snapshots as viewed from the side (*left* panel) and the top (*right* panel) of a weakly twisted (q = -0.75 rad a^{-1}) FR at t = 108. The FR is stable with no writhing and fails to exhibit the kink instability.

In this scenario, the values to all the parameters are kept identical to the first scenario except for the FR twist q which is set to $q = -0.75$ rad a^{-1} turns. Same as in the previous run, the FR is stopped when its axis r_0 is at z = 0. The FR emerges with limited upward expansion unlike the first run which involved excessive expansion upwards. The FR is in stable during its emergence and continues to be stable due to the reduced number of field line turns. This particular scenario was run the longest and at t = 108, the FR still remained stable. Due to this, the FR failed to produce the sigmoidal current sheet that was observed in the first scenario.

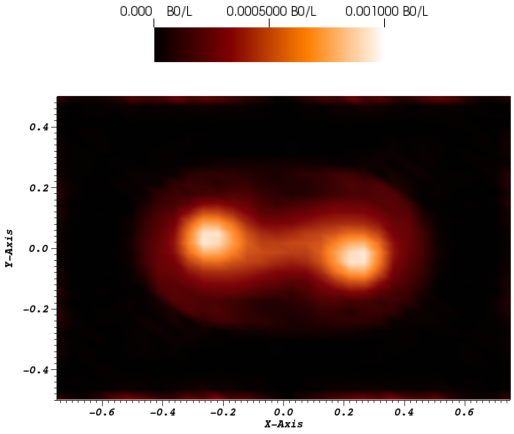

Figure 4.7: Horizontal cross section of the current density $|\mathbf{J}|$ at z = 0.25 and at time t = 108. No presence of a sigmoidal current sheet which suggests that the FR is stable.

Figure 4.6 shows a snapshot from t = 108 when the simulation was stopped. The FR shows very little expansion and does not show any writhing. Figure 4.7 shows the current density at z = 0.25. There are no signs of instability since there is no presence of a sigmoidal current sheet. The FR seems to be intact as most of the current density is concentrated in the FR axis. There is a very feint current layer around the FR due to its contact with the overlying fields similar to the one that appears in 4.4a.

Extreme twist (q = -1.75 rad a^{-1}) scenario

This scenario explores the emergence of an FR with extreme twist. Everything other than the twist is kept the identical to the previous two scenarios. The FR with q = –1.75 rad a^{-1} is transported into the corona and stopped when the FR axis r_0 is at z = 0.

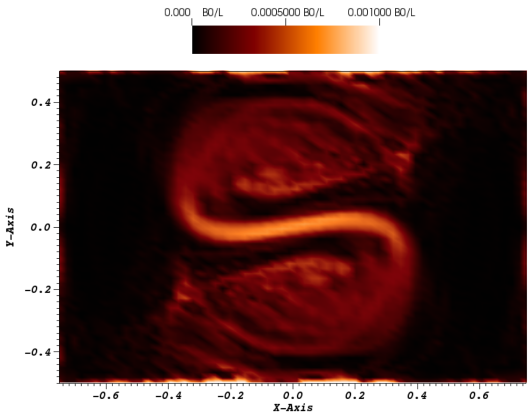

Figure 4.8: Horizontal cross section of the current density |**J**| at z = 0.45L. A current layer is formed in the center between the FR footpoints suggesting kink instability.

Figure 4.8 shows a horizontal cross section of the current density at z = 0.45L. The cross section is from t = 46 when the FR is clearly at the onset of kink instability as suggested by the strong current layer between the two legs of the FR.

A series of snapshots from the evolution can be found in Figure 4.9. The emerging FR becomes kink unstable midway through the emergence (4.9b). The top of the FR expands considerably faster compared to the previous scenarios. This excessive expansion causes the FR to exhibit significantly more writhing which leads to the onset of the kink instability very early in the emergence. The FR writhes more as seen in Figure 4.9c where the apex of the FR has writhing angle of more than 90°. This shows that when the field line twists exceed the threshold, the FR is highly unstable.

To explore further, the twist was increased to q = -2.25 rad a^{-1} and the effects from q = -1.75 rad a^{-1} was even more amplified with the emergence looking unphysical. The FR writhes and winds about its apex multiple times.

Additional scenario: Varying the FR stop height

Fan & Gibson (2004) performed a second run in which they stop the emerging FR prematurely to investigate if the previously kink unstable FR achieved an equilibrium state. The result was that an FR which has not reached the height at which it becomes unstable for a given twist (q = -1.25 rad a^{-1} in this case) will remain in equilibrium. This result by FG2004 is investigated for different "stop heights" (height at which the FR is stopped). They are checked for different twist values to find the critical twist needed for different stop heights.

As discussed in Section 4.1.2, the FR is stopped in its origin (r_0) as it reaches z = 0 (photospheric boundary), the value of r_0 = 0.375L at this point. The FR is now allowed to stop at much lower heights in the next set of simulation runs.

At first, the FR is stopped at a height of 0.225L for q = –1.25 rad a^{-1} turns. The expansion of the top of the FR is not as much as with the first scenario or the extreme twist scenario

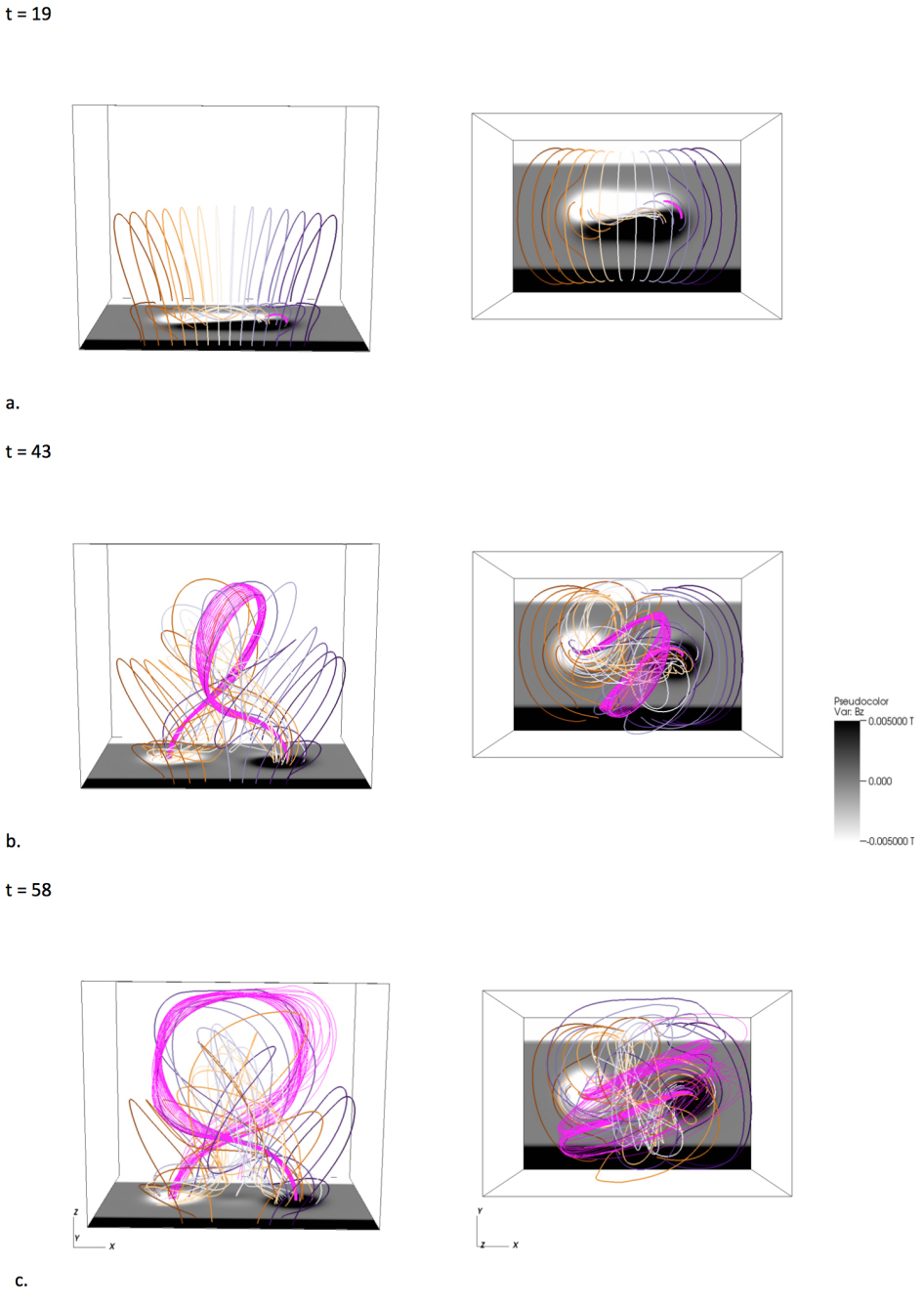

Figure 4.9: Snapshots as viewed from the side (*left* panels) and the top (*right* panels) of a highly twisted (q = -1.75 rad a^{-1}) FR. The FR is highly unstable and exhibits kink instability at t=43.

but however, the FR does become kink unstable but takes longer achieve it as the sigmoidal current layer is formed at a much later time than in the previous scenarios. Several runs are are made with different values of twist (two additional runs for every stop height by changing the twist by a factor of q = $\pm$0.25 rad a^{-1}) to get the critical twist for different heights considered. The simulations were run until the onset of instability and this can be seen in table 4.1. For a weakly twisted FR (q = -0.75 rad a^{-1}), it is stable at t = 108 and shows no signs of instability. Similarly, an extremely twisted FR (q = -2.25 rad a^{-1}) stopped at a very low height(0.165L) does not show any signs of instability. Results from the other stop heights are tabulated in Table 4.1. An FR stopped below 0.175L even with extreme twists is unable to exhibit any signs of instability and can be considered to be in equilibrium.

Table 4.1: Critical stop heights for varying amounts of twist

Twist (q rad a^{-1})	**Critical stop height**	**Time at the onset of instability**
- 0.75	No instability at 0.375L	FR stable at t = 108
- 1.0	0.275L	onset at t = 91
- 1.25	0.225L	onset at t = 88
- 1.5	0.200L	onset at t = 83
- 1.75	0.175L	onset at t = 78
- 2.25	No instability at 0.165L	FR stable at t = 103

It is important to remember that the amount of twist makes very little difference when the FR is stopped too low. 1.5 turns of twist produced no signs of instability below 0.200L and showed the same kind of stability exhibited by the FR in the second scenario. These simulations suggest that if the amount of twist is not converted to writhing then the result is an equilibrium.

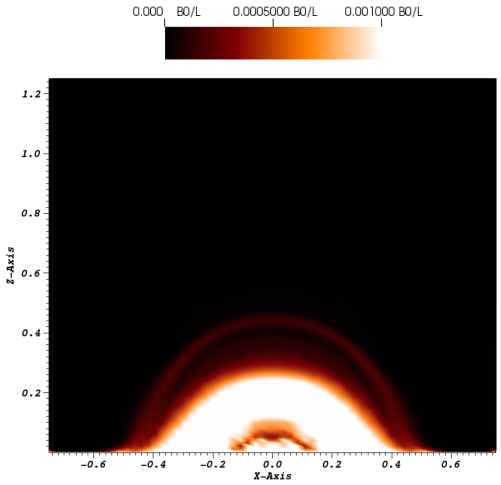

Figure 4.10: Cross section of the current density $|\mathbf{J}|$ at y = 0 for an FR with twist (q = -2.25 rad a^{-1}) stopped at 0.165L.

Figure 4.10 shows a vertical cross section of the current density $|\mathbf{J}|$ in the xz-plane at y = 0. The FR was allowed to emerge until it reached 0.165L (distance from the FR axis to the photospheric boundary z = 0). The FR is intact and shows no signs of instability at q = -1.25 rad a^{-1}. The current in the FR axis is the only major current in the corona.

4.4 Discussion

The work performed for this thesis uses the MFM to simulate an initially potential coronal magnetic field changing with a time-dependent photospheric boundary which transports a twisted magnetic flux rope. The FR emerging into the simulation domain is subject to instability in the form of helical kink (Chapter 2.4.2). The changes in the emerging FR that leads to the onset is of key importance in the field and is also one that is studied in FG2004. However, FG2004 use MHD in their study while the simulations and their results presented here utilize the MFM. The two models are compared for identical scenarios. But, the MFM is used to perform several more runs to see if results are produced, regardless of the changed configurations.

Throughout all runs, the FG model (Section 4.1.1) of the flux rope is used. Both the MHD and the MFM simulations use identical parameters which are discussed in the previous sections. However, the MFM uses an extra magneto-frictional coefficient which is chosen freely by the

modeler. The ad hoc nature of these parameter was discussed earlier in section 4.2.2. For the set of simulations run here, the coefficient is set to be $\nu = 10^{-13}$s/m^2. The speed of the emergence is constant ($V_m = 25$km/s) for all the scenarios. If the frictional coefficient is too high and the emergence speed is slow, it results in an unphysical evolution of the coronal arcade where the FR emerges into an arcade which does not evolve accordingly. This results in the FR not being able to emerge past the photospheric boundary.

Fan & Gibson report the detailed results for their simulation of a kinematically emerging FR in their publication (Fan & Gibson 2004). To summarize the results from the first run; there is a slow transport of twist into the corona until it reaches a threshold value of q = -1.25 rad a^{-1} field line turns making the FR highly unstable to the kink instability forming a thin "S" shaped current sheet. Titov & Demoulin (1999) found that FRs which exhibit this phenomena are more likely to erupt. In their second run, they stop the emergence of the FR prematurely and study the equilibrium of the FR which fails to become kink unstable.

The first scenario attempted to recreate the FG2004 model using the MFM. The results from that run show very similar results to the one presented by FG2004.

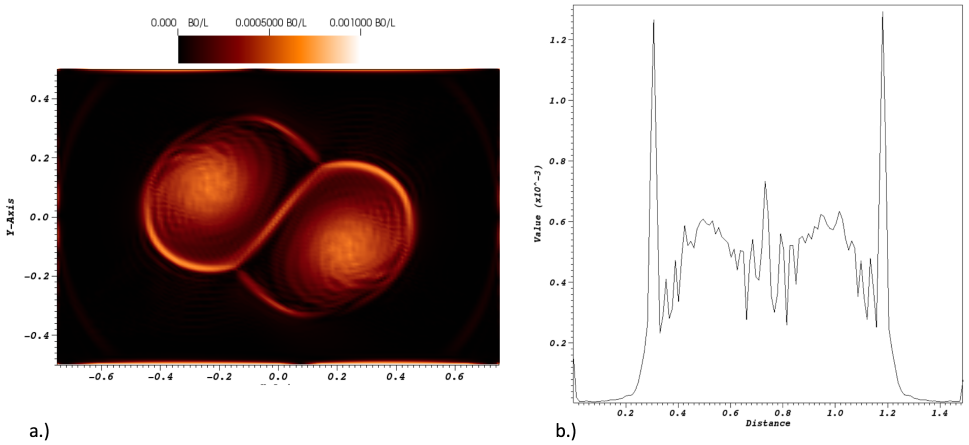

Figure 4.11: a.) Horizontal cross section of the current density |**J**| at z = 0.25L. b.) Magnitude of the current density where the peaks denote the sigmoidal current layer across the FR footpoints

In the MFM simulations, the "S" shape current sheet is due to the kink instability and its dynamic nature. During the onset of KI, the twisted magnetic field lines close to the photosphere and the neighboring field lines which are line tied are discontinuous. This behavior of magnetic field lines is described by Fan & Gibson using MHD. They suggest that these discontinuities could be where reconnection and heating is the strongest and therefore appears as a bright sigmoid. In the MFM, there is a topological change in the magnetic fields but it can neither produce reconnection nor heating due to the nature of the model. However, since there is a presence of a non-zero diffusivity term in the MFM, these discontinuities can be modeled and analyzed.

Figure 4.11a shows horizontal cross sections of the current density at z = 0.25L. The peaks in the magnitude of the current density is shown in 4.11b. The sigmoidal current layer is the strongest concentration of current in the corona during the onset of kink instability. In both the FG2004 simulation and the ones presented here, the sigmoid appears for a very short time during the onset of instability. While explaining short X-ray brightening (Moore et al 2001) which have a sigmoidal geometry, the model does not explain the sigmoids which lasts days in the corona (Leamon et al 2003).

The kink instability is one of the reasons for these topological changes and can be seen clearly in the attached movie clip (label: FRemergence3D.mp4) or the snapshots in Figure 4.3 and 4.9.

The top down view of the simulation box helps identify these changes as the field lines in the photospheric boundary twist around the footpoints of the emerged FR.

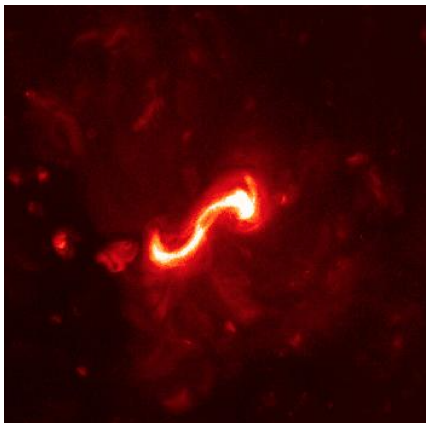

Figure 4.12: Bright sigmoid observed by Hinode X-Ray Telescope (XRT) during the development before its eruption on February 12,2007. (credits: *http://solar.physics.montana.edu/press/XRTSigmoid.html*)

A sigmoid that formed during the onset of the February 12, 2007 eruption is seen in Figure 4.12, which was observed using the Hinode X-Ray telescope (XRT). Comparing it to the results presented here; The formation of a thin current sheet can be seen in Figure 4.11a, it has the sigmoidal shape as suggested by FG2004. The formation of the current sheet at the onset of kink instability is suggested in their discussion. An earlier letter (Fan & Gibson 2003) describes this further. The formation of the current sheet also suggests reconnection of the magnetic field lines during the onset of instability. The current sheet is formed due to the "squeezing" of opposing magnetic field lines when they come together (Parker 1958). Details of this phenomena can be found in a number of classic textbooks(e.g: Aschwanden 2005).

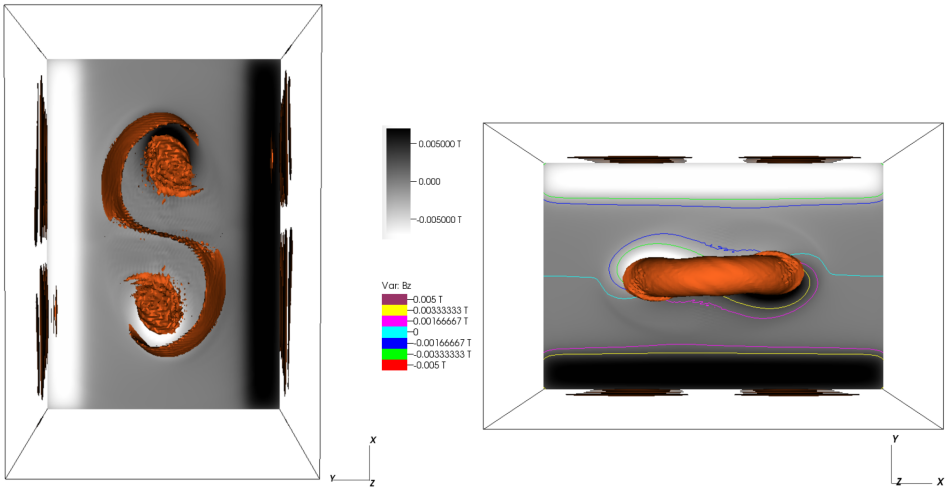

(a) Iso-sruface of |**J**| at t = 79 (b) Iso-sruface of |**J**| at t = 40

Figure 4.13: (a) Iso-surface of the current density showing the formation of the sigmoidal current layer at the onset of kink instability. (b) Contour plot of the vertical magnetic field (B_z) shown with the Iso-surface of the FR current density.

Figure 4.13 shows two iso-surface plots of the current density at different times for the first scenario (q = -1.25 rad a^{-1}). The iso-surface level is set to 0.0005 B_0 L^{-1}. Figure 4.13b shows the current density in the corona which is concentrated at the central axis of the FR at t = 40. Contour lines of the magnetic field B_z are drawn on the photospheric boundary to show the footpoints of the FR divided by the Polarity inversion line (PIL)(a line dividing the positive and negative polarities of the magnetic field in an active region). Figure 4.13a shows the same FR at t =79 when it is kink unstable. The current in the corona is concentrated in a sigmoidal

shape around the FR footpoints. The central part of the current sheet crosses the PIL as it is seen in X-ray observations (Figure 4.12) in a bipolar magnetic region. The results are close to FG2004, but it is necessary to have the best spatial resolutions in order to resolve the current layer and to measure its magnitude.

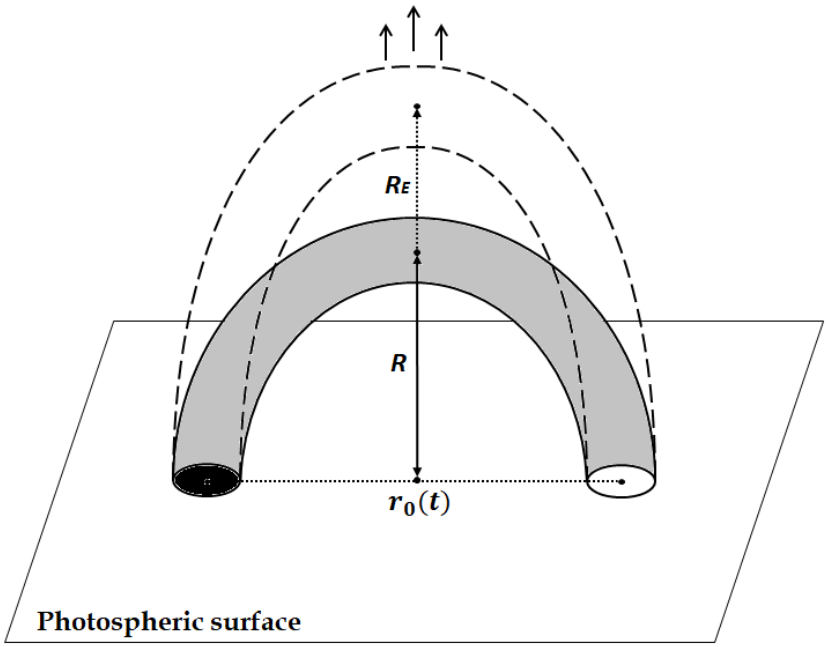

Figure 4.14: Illustration explaining the FR expansion. R is the radius of the torus and R_E is the amount of expansion of the FR axis from its original path)

In all the runs except when the FR has very little twist or is stopped too early, the top of the tube experiences an upward force independent of the boundary driving speed. These observations are noted by Fan & Gibson (2004, 2007, 2010) where they describe an FR showing features of torus instability even when the conditions for TI are not part of the initial conditions of the experiment. This would mean that the FR model proposed by Fan & Gibson is inherently torus unstable. According to Karlicky & Kliem (2010), a kink unstable FR can be perturbed radially causing it to expand (Fan & Gibson 2007, 2010 (two-part report)). This expansion, however, assists the FR at the onset of helical kink instability as more writhe is converted to twist leading to instability. Since the FR is line tied, the expansion is noticed at its leading edge. For the runs discussed here, the expansion assists in the loss of stability.

It is possible to measure the upward expansion that the FR experiences through line-out plots from the simulation domain and measuring them against the initial structure of the flux rope torus. The process of expansion if illustrated in Figure 4.14 where R_E is how much the top of the FR has changed from the original shape of the FR. Figure 4.15 shows the FR expansion plotted against the twist. It can be seen that the FR with higher twists tend to expand more.

The height at which the FR is stopped also plays a key role in the onset of instability. The fourth scenario works on addressing that and it is seen from Table 4.1 that, the height of the flux rope in the photosphere is crucial to the kink instability. A similar line out plot is used to compare the influence of stop height on the upward expansion of the FR. The results for the five different stop heights are given in Figure 4.16

The slow energization of the coronal magnetic field from a potential state is addressed using MFM. The coronal magnetic field arcade is current free in its initial state and is energized by the emergence of the FR which carries current concentrated in its axis. However, at the onset

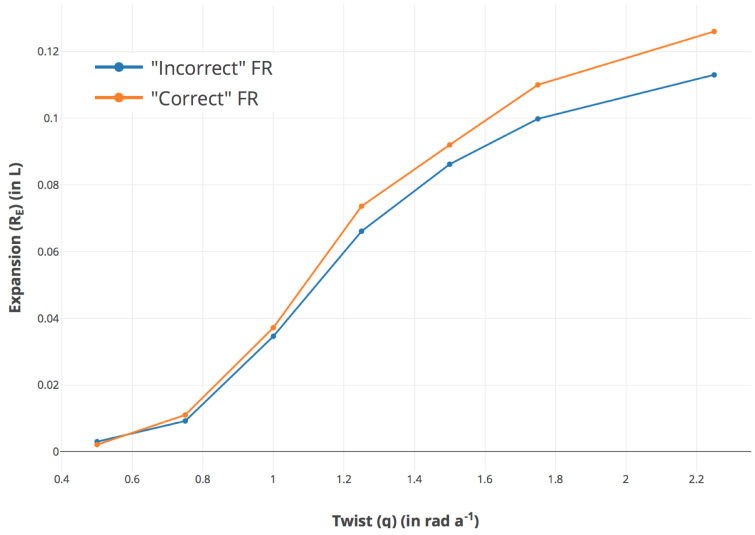

Figure 4.15: A comparative plot between the "incorrect" and "correct" FRs showing the role of twist in the expansion of the FR. Stop height is fixed at 0.350L for all runs.

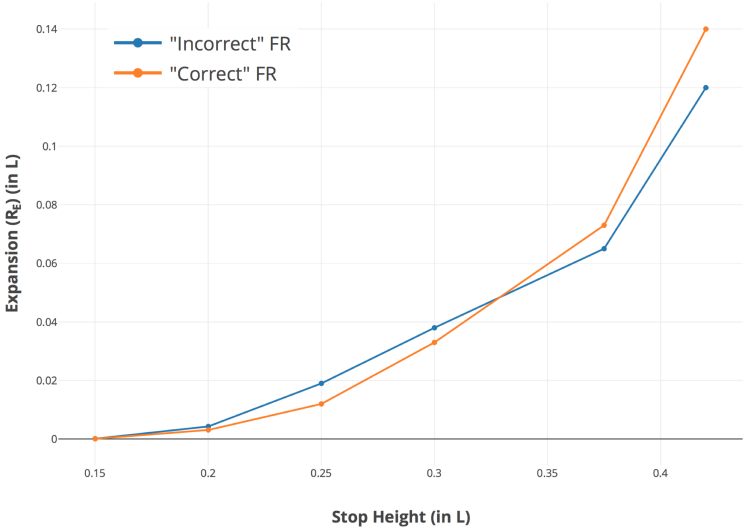

Figure 4.16: plot showing the importance of the stop height(height the FR is allowed to emerge into the corona) in the leading edge expansion of the FR. q = -1.25 rad a^{-1} throughout all runs.

of kink instability, a new current layer is formed which is sigmoidal in shape which becomes the most dominant current in the corona.

Snapshots from the movie clip of the the emergence in the yz – plane can be seen in Figure 4.17. Analyzing these snapshots, it is possible to see the changes in current distribution in the corona as the FR emerges. Figure 4.17a is the initial potential field configuration with no current. This changes gradually with the slow transportation of the FR into the corona. Figure 4.17b shows the FR at t =20 and the feint current layer on the top where the FR comes in contact with the coronal arcade can be seen very clearly. At t = 79 (Figure 4.17d) at the onset of kink instability, the most dominant current is in a layer at in the middle which at z = 0.25 appeared to be a sigmoidal current layer.

The movie clip (label: FRenergization2D.mpg) attached to this thesis shows the full emergence process in the yz-plane. The coronal magnetic field becomes energized with the introduction of a current carrying FR. As seen in the movie clip, the cross section shows that the strongest current density is the current that flow through the FRs central region. There is also a small

presence of current between the FR and the outer coronal field arcade. As the FR emerges further and starts to become kink unstable and develops writhing, the current layer in the middle (sigmoidal from the z=0.25 slide in Figure 4.11a) becomes the new dominant feature of the current distribution in the corona.

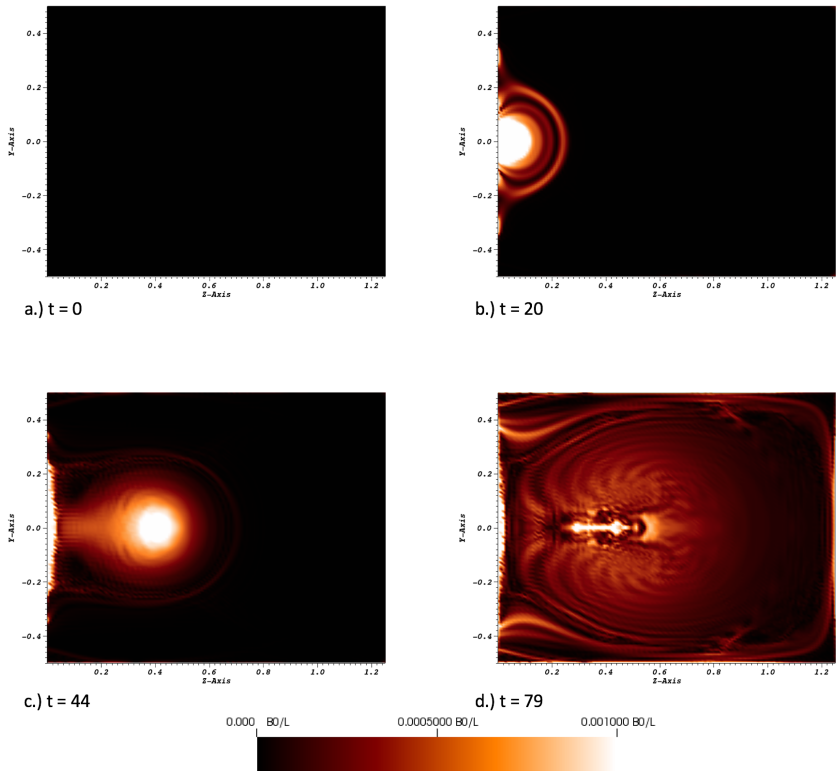

Figure 4.17: vertical cross sections of the current density $|\mathbf{J}|$ in the yz-plane for the $q = -1.25\,\mathrm{rad\,a^{-1}}$ scenario. A movie clip of the slow evolution of the current in the corona is available with this e-thesis (label: FRenergization2D.mpg)

4.4.1 Correction to Fan & Gibson simulations

A close investigation into the FG2004 model showed a an error in one of their calculations. The error occurs in Equation 4.4,

$$\varpi = (r^2 + R^2 - 2rR\sin^2\theta)^{\frac{1}{2}}.$$

According to trigonometric identities, the above equation should have been

$$\varpi = (r^2 + R^2 - 2rR\sin\theta)^{\frac{1}{2}} \tag{4.8}$$

The $\sin^2\theta$ present in the original equation is thus incorrect and it was later corrected by Fan in the subsequent publication in 2005. The changes that can happen to the simulations due to this particular correction is discussed in later sections. It is also important to compare the results after the correction with the results before it.

The expression affects the distance from the FR axis to the origin. This could make the FR to expand more on its leading edge. As discussed in 2.4.1, a toroidal FR is torus unstable if there is a change in the distance from the toroidal axis to the origin. The new "correct" torus is simulated through the same conditions as the FG2004 torus.

4.4.2 "Correct" FR scenario

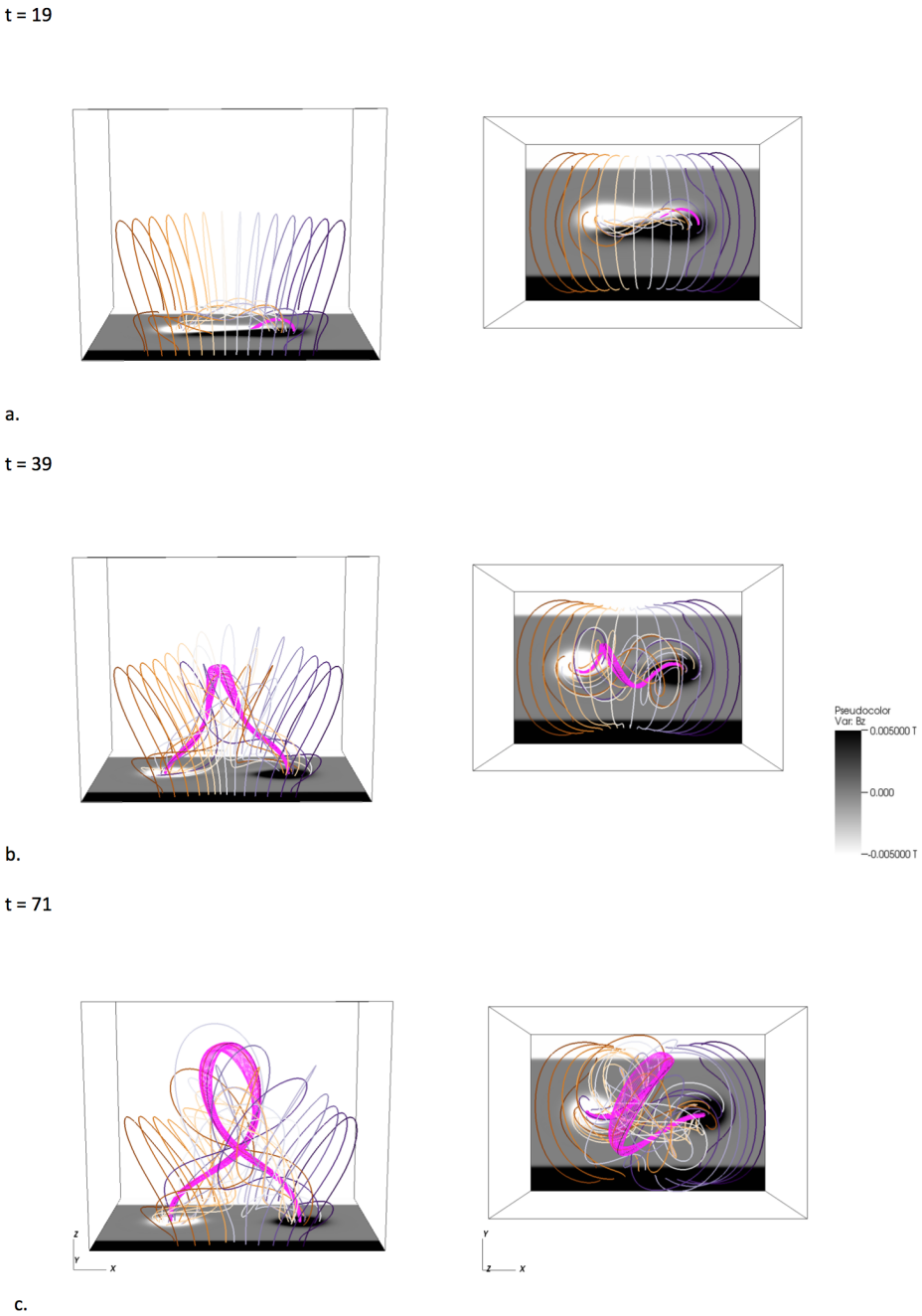

Figure 4.18: Snapshots from the simulation of the fixed equation showing the emergence of the flux tube into the coronal arcade at a much faster rate.

Using the "correct" expression (Equation 4.8), a new set of simulations are made. The runs are identical to the ones performed in the first four scenarios. The first scenario in particular is studied carefully. It is to help compare the changes in the simulation using MFM to the results of FG2004.

Snapshots from the recreation of the first scenario can be seen in Figure 4.18. It is noticeable that the FR undergoes more expansion in its top part. This causes the FR to writhe more and leads to the onset of instability much faster than the first scenario. The FR is then simulated for other scenarios and plots comparing the incorrect FR to the fixed FR are made. These plots can be seen in Figure 4.15 & 4.16 show that the "correct" FR behaves differently than

the "incorrect" FR. The plot in Figure 4.15 shows the expansion with respect to the twist of the flux rope. It is seen that both the FR models experience similar expansions at low twists and the change is more noticeable for FRs with high twist.

During the onset of kink instability, a narrow current sheet is formed similar to the other scenarios. This could also be seen in the magnetic field lines in Figure 4.18, the topologies of which exhibit a twisting around the emerging flux rope as seen in Figure 4.18c.

A number of extended simulation runs are made to analyze the behavior of the "correct" flux rope at higher twist values and also for different stop heights. The FR behavior is consistent with the curves in Figures 4.15 & 4.16; showing reduced stability at higher values of twist and also at higher stop heights. A comparative analysis of this is found in section 4.4.3.

4.4.3 Comparing the models

With the data collected from several numerical runs, it is possible to make conclusions on the MFM using the Fan & Gibson model. These conclusions are made by comparing and discussing the results in MFM and MHD (simulations by Fan & Gibson, 2004).

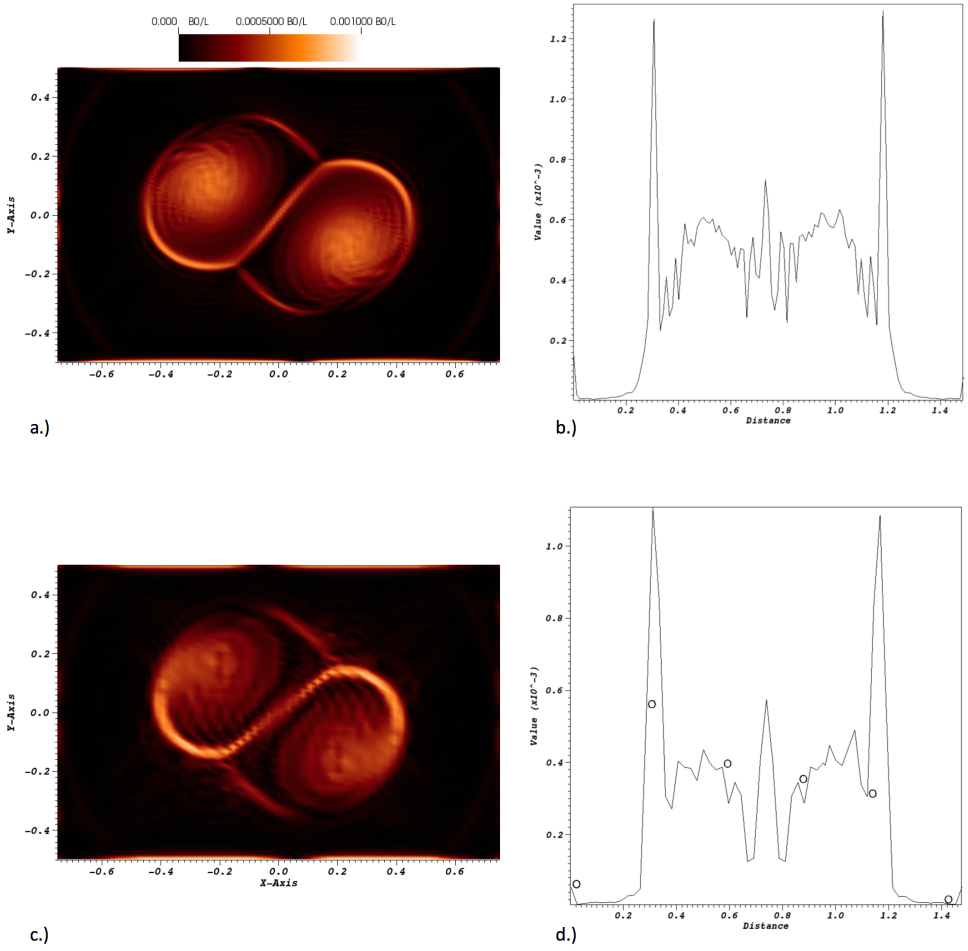

Figure 4.19: (a) Plot showing the formation of a sigmoidal current sheet for the "incorrect" FR with a field line twist q = –1.25 rad a^{-1} scenario & (b) shows the magnitude of the current density across the y = 0 line. (c) Plot showing the formation of a sigmoidal current sheet for the "correct" FR with a field line twist q = –1.25 rad a^{-1} and (d) shows the magnitude of the current density in the y=0 line.

The toroidal FR itself is identical in both MHD and MFM. However, the change occurs when the

MFM also considers a "correct" expression. As described in the above sections 4.3.2 and 4.4.2, the most noticeable difference between the "correct" and the "incorrect" FRs is the expansion at their leading part. Examining the plots 4.15 and 4.16, It is seen that the expansion in both the models for the q = –1.25 rad a^{-1} and a stop height 0.375L is similar. The "correct" FR shows slightly more expansion as seen by comparing t = 44 in Figure 4.3b and t = 39 of Figure 4.18b. These changes are more pronounced when the twists are extreme. The "correct" FR shows a higher degree of expansion for all cases considered.

The consequences to the FR from changing the height until which it is allowed to emerge is seen in Figure 4.16. The plot compares the "incorrect" FR with the "correct" FR. A few things can be noted from this comparison; The "correct" FR is more stable at smaller stop heights and substantially more unstable at higher stop heights. At a stop height of 0.375L, the "correct" FR shows greater expansion than its counterpart.

Figure 4.19a shows a current sheet from the first scenario with the "incorrect" FR. Comparing it with Figure 4.19c, which is the recreation of the same FR with the "fixed equation, it shows many similarities to the current sheet in 4.19a. The similarities can also be seen when comparing the current densities plotted at the time of the onset of instability. Figure 4.19b and Figure 4.19d show these plots. The magnitude of the current densities in both these cases are roughly similar with three distinct peaks in current density across the y = 0 line in Figures 4.19a and 4.19c. The two peaks on the sides are from the bright layers of current around the footpoints while the peak in the middle is from the current layer which passes the PIL.

The "correct" scenario although showing more expansion and writhing has a smaller current in these peaks which could be due to the lower resolution of the "correct" simulation run. FG2004 point out the differences between current sheets produced in a high resolution run with a low resolution run. The higher resolution run produced or rather showed higher peak values. The conclusion was that the magnitude in these lines linearly increase with the resolution.

As for the changes in the coronal magnetic field; They are similar yet again. Figure 4.18c shows a snapshot of the same FR as in the first scenario at the onset of instability. The "correct" FR exhibits more writhing and the angle of writhing exceeds 90° of the "incorrect" FR. They are most similar midway through the emergence (Figures 4.3b & 4.18b), where the arcades look very much alike with the emerging FR. One can compare the results side by side and visually notice the similarities. However, due to the slight difference in how they evolve, the "correct" FR writhes more than the "incorrect" FR and becomes kink unstable at an earlier time.

4.5 Moving forward

The results presented in the above sections from studying the ideal kink instability in a flux rope torus that emerges into a pre-existing coronal arcade are mostly comparable to the FG2004. The magneto-frictional method (MFM) which was employed for for this study has shown that it is a capable model to study solar eruptive events. Choosing the right parameters and an accurate boundary condition is essential for the success of the MFM. If it can be chosen to be accurate, the model can be used in data-driven studies. Applying the MFM in such investigations of active regions to produce eruptive flux ropes and filaments is the next logical step in the future. Active work has been done in the space physics research group at the University of Helsinki to provide the necessary boundary conditions so that the data-driven objectives could be met. The long term goal of the research group is to create a modeling pipeline for a space weather chain. This would involve modeling from the photospheric and coronal evolution of the magnetic fields and the formation and evolution of eruptive phenomena through the upper corona and into the

heliosphere. By combining a variety of models that have been tested here to produce a chain can be very crucial in achieving real-time space weather predictions.

The continuation of the work presented here in this thesis is identifying and studying different solutions to the force-free equation. These solutions can then be applied in studying the evolution of toroidal flux ropes in the upper corona. The work would help identify characteristics of different flux ropes (Lundquist, Gold-Hoyle, Fan-Gibson, etc.,) in the heliosphere. The aim is to finally integrate toroidal flux ropes into the heliospheric space weather prediction model EUFHORIA (EUropean Heliospheric FORecasting Information Asset).

Acknowledgements

This work is the culmination to a year of scientific study and learning. A journey driven by adventurous exploration of a subject that has left me flabbergasted on more than a few occasions. However, this journey would not have been possible if it were not for the wonderful people who led me to the gates and helped me walk through it. I would like to take this opportunity to thank each and every one of them.

I would like to express my deepest appreciation to Professor Koskinen who has been a great figure of inspiration since starting my studies here. I would also like to thank him for his guidance, without which, I would have not had the opportunity to delve deep into the field of space science.

I am also extremely grateful to Professor Kilpua who admitted me into her research group and provided me with her endless support and trust. Her knowledge as a scientist and as an educator has helped me grow and learn invaluable lessons over the past two years. If it were not for her confidence in my ability, I would not have had the chance to grow as a researcher and experience science the way I did.

I would also like to thank Dr. Pomoell who I worked with closely. His excellence and foresight in the field is unparalleled and I was lucky to have had the chance to work under his supervision. His straightforwardness and timely advice have helped me improve as a researcher and as a person in general. Above all, I appreciate his concern and good will at times of need.

In addition, a thank you to the members of the space research group for all their help. I would like to thank Matti, Erkka and Erika in special as they guided me in easing through the university courses.

Finally, I would like to sincerely thank my parents who have supported me emotionally and financially. None of this would have been possible without their love and support. My thanks also goes to my dear friend Anastasiia who has been my moral support and a source of light during dark times.

Bibliography

Alexander, D., Liu, R. & Gilbert, H. R. (2006), 'Hard X-Ray Production in a Failed Filament Eruption', *The Astrophysical Journal* **653**, 719–724.

Alissandrakis, C. E. (1981), 'On the computation of constant alpha force-free magnetic field', *Astronomy and Astrophysics Journal* **100**, 197–200.

Amari, T., Canou, A. & Aly, J.-J. (2014), 'Characterizing and predicting the magnetic environment leading to solar eruptions', *Nature Physics* **514**, 465–469.

Amari, T., Luciani, J. F. & Aly, J. J. (2005), 'Non-Current-free Coronal Closure of Subphotospheric MHD Models', *The Astrophysical Journal* **629**, L37–L40.

Amari, T., Luciani, J. F., Aly, J. J., Mikic, Z. & Linker, J. (2003*a*), 'Coronal Mass Ejection: Initiation, Magnetic Helicity, and Flux Ropes. I. Boundary Motion-driven Evolution', *The Astrophysical Journal* **585**, 1073–1086.

Amari, T., Luciani, J. F., Aly, J. J., Mikic, Z. & Linker, J. (2003*b*), 'Coronal Mass Ejection: Initiation, Magnetic Helicity, and Flux Ropes. II. Turbulent Diffusion-driven Evolution', *The Astrophysical Journal* **595**, 1231–1250.

Antiochos, S. K., DeVore, C. R. & Klimchuk, J. A. (1999), 'A Model for Solar Coronal Mass Ejections', *The Astrophysical Journal* **510**, 485–493.

Anzer, U. (1968), 'The Stability of Force-Free Magnetic Fields with Cylindrical Symmetry in the Context of Solar Flares', *Solar Physics* **3**, 298–315.

Anzer, U. (1972), 'A Method to Calculate Electric Currents in Quiescent Prominences', *Solar Physics* **24**, 324–335.

Archontis, V. & Hood, A. W. (2012), 'Magnetic flux emergence: a precursor of solar plasma expulsion', *Astronomy and Astrophysics Journal* **537**, A62.

Archontis, V., Hood, A. W., Savcheva, A., Golub, L. & Deluca, E. (2009), 'On the Structure and Evolution of Complexity in Sigmoids: A Flux Emergence Model', *The Astrophysical Journal* **691**, 1276–1291.

Archontis, V., Moreno-Insertis, F., Galsgaard, K., Hood, A. & O'Shea, E. (2004), 'Emergence of magnetic flux from the convection zone into the corona', *Astronomy and Astrophysics Journal* **426**, 1047–1063.

Aschwanden, M. J. (2005), *Physics of the Solar Corona. An Introduction with Problems and Solutions (2nd edition)*.

Aulanier, G., Srivastava, N. & Martin, S. F. (2000), 'Model Prediction for an Observed Filament', *The Astrophysical Journal* **543**, 447–456.

Aulanier, G., Török, T., Démoulin, P. & DeLuca, E. E. (2010), 'Formation of Torus-Unstable Flux Ropes and Electric Currents in Erupting Sigmoids', *The Astrophysical Journal* **708**, 314–333.

Bateman, G. (1978), *MHD instabilities*.

Baty, H. & Heyvaerts, J. (1996), 'Electric current concentration and kink instability in line-tied coronal loops.', *Astronomy and Astrophysics Journal* **308**, 935–950.

Berger, M. A. (1984), 'Rigorous new limits on magnetic helicity dissipation in the solar corona', *Geophysical & Astrophysical Fluid Dynamics* **30**(1-2), 79–104.

Berger, M. A. (1999), 'Introduction to magnetic helicity.', *Plasma Physics and Controlled Fusion* **41**, B167–B175.

Berger, M. A. & Field, G. B. (1984), 'The topological properties of magnetic helicity', *Journal of Fluid Mechanics* **147**, 133–148.

Borrero, J. M., Asensio Ramos, A., Collados, M., Schlichenmaier, R., Balthasar, H., Franz, M., Rezaei, R., Kiess, C., Orozco Suárez, D., Pastor, A., Berkefeld, T., von der Lühe, O., Schmidt, D., Schmidt, W., Sigwarth, M., Soltau, D., Volkmer, R., Waldmann, T., Denker, C., Hofmann, A., Staude, J., Strassmeier, K. G., Feller, A., Lagg, A., Solanki, S. K., Sobotka, M. & Nicklas, H. (2016), 'Deep probing of the photospheric sunspot penumbra: no evidence of field-free gaps', *Astronomy and Astrophysics Journal* **596**, A2.

Boyd, T. J. M. & Sanderson, J. J. (2003), *The Physics of Plasmas*.

Brueckner, G. E., Delaboudiniere, J.-P., Howard, R. A., Paswaters, S. E., St. Cyr, O. C., Schwenn, R., Lamy, P., Simnett, G. M., Thompson, B. & Wang, D. (1998), 'Geomagnetic storms caused by coronal mass ejections (cmes): March 1996 through june 1997', *Geophysical Research Letters* **25**(15), 3019–3022.

Burlaga, L. F., Klein, L., Sheeley, Jr., N. R., Michels, D. J., Howard, R. A., Koomen, M. J., Schwenn, R. & Rosenbauer, H. (1982), 'A magnetic cloud and a coronal mass ejection', *Journal of Geophysical Research (Space Physics)* **9**, 1317–1320.

Burlaga, L., Sittler, E., Mariani, F. & Schwenn, R. (1981), 'Magnetic loop behind an interplanetary shock - Voyager, Helios, and IMP 8 observations', *Journal of Geophysical Research (Space Physics)* **86**, 6673–6684.

Chen, J. (2012), 'Structure of non-force-free magnetic flux ropes in an ambient medium', *The Astrophysical Journal* **761**(2), 179.

Cheung, M. C. M. & DeRosa, M. L. (2012), 'A Method for Data-driven Simulations of Evolving Solar Active Regions', *The Astrophysical Journal* **757**, 147.

Chiu, Y. T. & Hilton, H. H. (1977), 'Exact Green's function method of solar force-free magnetic-field computations with constant alpha. I - Theory and basic test cases', *The Astrophysical Journal* **212**, 873–885.

Cho, K. S., Park, S. H., Marubashi, K., Gopalswamy, N., Akiyama, S., Yashiro, S., Kim, R. S. & Lim, E. K. (2013), 'Comparison of Helicity Signs in Interplanetary CMEs and Their Solar Source Regions', *Solar Physics* **284**(1), 105–127.

Chodura, R. & Schlueter, A. (1981), 'A 3D code for MHD equilibrium and stability', *Journal of Computational Physics* **41**, 68–88.

Chui, A. Y. K. & Moffatt, H. K. (1995), 'The Energy and Helicity of Knotted Magnetic Flux Tubes', *Proceedings of the Royal Society of London Series A* **451**, 609–629.

Cohen, O., Sokolov, I. V., Roussev, I. I., Arge, C. N., Manchester, W. B., Gombosi, T. I., Frazin, R. A., Park, H., Butala, M. D., Kamalabadi, F. & Velli, M. (2007), 'A Semiempirical Magnetohydrodynamical Model of the Solar Wind', *The Astrophysical Journal* **654**, L163–L166.

Cravens, T. (2004), *Physics of Solar System Plasmas*, Cambridge Atmospheric and Space Science Series, Cambridge University Press.

Cremades, H. & Bothmer, V. (2004), 'On the three-dimensional configuration of coronal mass ejections', *Astronomy and Astrophysics Journal* **422**, 307–322.

De Wijn, A. G., Stenflo, J. O., Solanki, S. K. & Tsuneta, S. (2009), *Small-scale solar magnetic fields*, Vol. 144.

Démoulin, P. & Aulanier, G. (2010), 'Criteria for Flux Rope Eruption: Non-equilibrium Versus Torus Instability', *The Astrophysical Journal* **718**, 1388–1399.

Domingo, V., Fleck, B. & Poland, A. I. (1995), 'The SOHO Mission: an Overview', *Solar Physics* **162**, 1–37.

Dungey, J. W. (1961), 'Interplanetary Magnetic Field and the Auroral Zones', *Physical Review Letters* **6**, 47–48.

Edlén, B. (1943), 'Die Deutung der Emissionslinien im Spektrum der Sonnenkorona. Mit 6 Abbildungen.', **22**, 30.

Fan, Y. (2001*a*), 'Nonlinear Growth of the Three-dimensional Undular Instability of a Horizontal Magnetic Layer and the Formation of Arching Flux Tubes', *The Astrophysical Journal* **546**, 509–527.

Fan, Y. (2001*b*), 'The Emergence of a Twisted Ω-Tube into the Solar Atmosphere', *The Astrophysical Journal* **554**, L111–L114.

Fan, Y. (2004), 'Magnetic Fields in the Solar Convection Zone', *Living Reviews in Solar Physics* **1**, 1.

Fan, Y. (2005), 'Coronal Mass Ejections as Loss of Confinement of Kinked Magnetic Flux Ropes', *The Astrophysical Journal* **630**, 543–551.

Fan, Y. (2010), 'On the Eruption of Coronal Flux Ropes', *The Astrophysical Journal* **719**, 728–736.

Fan, Y. & Gibson, S. E. (2003), 'The Emergence of a Twisted Magnetic Flux Tube into a Preexisting Coronal Arcade', *The Astrophysical Journal* **589**, L105–L108.

Fan, Y. & Gibson, S. E. (2004), 'Numerical Simulations of Three-dimensional Coronal Magnetic Fields Resulting from the Emergence of Twisted Magnetic Flux Tubes', *The Astrophysical Journal* **609**, 1123–1133.

Fan, Y. & Gibson, S. E. (2006), 'On the Nature of the X-Ray Bright Core in a Stable Filament Channel', *The Astrophysical Journal* **641**, L149–L152.

Fan, Y. & Gibson, S. E. (2007), 'Onset of Coronal Mass Ejections Due to Loss of Confinement of Coronal Flux Ropes', *The Astrophysical Journal* **668**, 1232–1245.

Feng, X., Yang, L., Xiang, C., Jiang, C., Ma, X., Wu, S. T., Zhong, D. & Zhou, Y. (2012), 'Validation of the 3D AMR SIP-CESE Solar Wind Model for Four Carrington Rotations', *Solar Physics* **279**, 207–229.

Filippov, B., Martsenyuk, O., Srivastava, A. K. & Uddin, W. (2015), 'Solar Magnetic Flux Ropes', *Journal of Astrophysics and Astronomy* **36**, 157–184.

Forbes, T. G. & Isenberg, P. A. (1991), 'A catastrophe mechanism for coronal mass ejections', *The Astrophysical Journal* **373**, 294–307.

Forbes, T. G., Linker, J. A., Chen, J., Cid, C., Kóta, J., Lee, M. A., Mann, G., Mikić, Z., Potgieter, M. S., Schmidt, J. M., Siscoe, G. L., Vainio, R., Antiochos, S. K. & Riley, P. (2006), 'CME Theory and Models', *Space Science Reviews* **123**, 251–302.

Goedbloed, J. & Poedts, S. (2004), *Principles of Magnetohydrodynamics: With Applications to Laboratory and Astrophysical Plasmas*, Cambridge University Press.

Gopalswamy, N., Lara, A., Yashiro, S., Kaiser, M. L. & Howard, R. A. (2001), 'Predicting the 1-AU arrival times of coronal mass ejections', *Journal of Geophysical Research (Space Physics)* **106**, 29207–29218.

Green, L. M., Kliem, B., Török, T., Van Driel-Gesztelyi, L. & Attrill, G. D. R. (2007), 'Transient coronal sigmoids and rotating erupting flux ropes', *Solar Physics* **246**(2), 365–391.

Guo, Y., Ding, M. D., Schmieder, B., Li, H., Trk, T. & Wiegelmann, T. (2010), 'Driving mechanism and onset condition of a confined eruption', *The Astrophysical Journal Letters* **725**(1), L38.

Hassler, D. M., Dammasch, I. E., Lemaire, P., Brekke, P., Curdt, W., Mason, H. E., Vial, J.-C. & Wilhelm, K. (1999), 'Solar Wind Outflow and the Chromospheric Magnetic Network', *Science* **283**, 810.

Hayashi, K. (2005), 'Magnetohydrodynamic Simulations of the Solar Corona and Solar Wind Using a Boundary Treatment to Limit Solar Wind Mass Flux', *The Astrophysical Journals* **161**, 480–494.

Heyvaerts, J. & Priest, E. R. (1984), 'Coronal heating by reconnection in DC current systems - A theory based on Taylor's hypothesis', *Astronomy and Astrophysics Journal* **137**, 63–78.

Hood, A. W. & Priest, E. R. (1981), 'Critical conditions for magnetic instabilities in force-free coronal loops', *Geophysical and Astrophysical Fluid Dynamics* **17**, 297–318.

House, L. L. & Berger, M. A. (1987), 'The ejection of helical field structures through the outer corona', *The Astrophysical Journal* **323**, 406–413.

Inoue, S., Hayashi, K., Magara, T., Choe, G. S. & Park, Y. D. (2015), 'Magnetohydrodynamic Simulation of the X2.2 Solar Flare on 2011 February 15. II. Dynamics Connecting the Solar Flare and the Coronal Mass Ejection', *The Astrophysical Journal* **803**, 73.

Isenberg, P. A. & Forbes, T. G. (2007), 'A Three-dimensional Line-tied Magnetic Field Model for Solar Eruptions', *The Astrophysical Journal* **670**, 1453–1466.

Janvier, M., Aulanier, G., Pariat, E. & Démoulin, P. (2013), 'The standard flare model in three dimensions. III. Slip-running reconnection properties', *Astronomy and Astrophysics Journal* **555**, A77.

Ji, H.-s., Song, M.-t., Zhang, Y.-a. & Song, S.-m. (2003), 'The horizontal and vertical electric currents in three solar active regions and their relations with flares', **27**, 79–88.

Jian, L., Russell, C. T., Luhmann, J. G. & Skoug, R. M. (2006*a*), 'Properties of Interplanetary Coronal Mass Ejections at One AU During 1995 2004', *Solar Physics* **239**, 393–436.

Jian, L., Russell, C. T., Luhmann, J. G. & Skoug, R. M. (2006*b*), 'Properties of Stream Interactions at One AU During 1995 2004', *Solar Physics* **239**, 337–392.

Jiang, C. & Feng, X. (2012), 'A New Implementation of the Magnetohydrodynamics-relaxation Method for Nonlinear Force-free Field Extrapolation in the Solar Corona', *The Astrophysical Journal* **749**, 135.

Jiang, C., Wu, S. T., Feng, X. & Hu, Q. (2014), 'Formation and Eruption of an Active Region Sigmoid. I. A Study by Nonlinear Force-free Field Modeling', *The Astrophysical Journal* **780**, 55.

Jiang, C., Wu, S. T., Feng, X. & Hu, Q. (2016), 'Data-driven magnetohydrodynamic modelling of a flux-emerging active region leading to solar eruption', *Nature Communications* **7**, 11522.

Karlický, M. & Kliem, B. (2010), 'Reconnection of a Kinking Flux Rope Triggering the Ejection of a Microwave and Hard X-ray Source I. Observations and Interpretation', *Solar Physics* **266**, 71–89.

Kazachenko, M. D., Fisher, G. H., Welsch, B. T., Liu, Y. & Sun, X. (2015), 'Photospheric Electric Fields and Energy Fluxes in the Eruptive Active Region NOAA 11158', *The Astrophysical Journal* **811**, 16.

Klein, L. W. & Burlaga, L. F. (1982), 'Interplanetary magnetic clouds at 1 au', *Journal of Geophysical Research (Space Physics)* **87**, 613–624.

Kliem, B., Su, Y. N., van Ballegooijen, A. A. & DeLuca, E. E. (2013), 'Magnetohydrodynamic Modeling of the Solar Eruption on 2010 April 8', *The Astrophysical Journal* **779**, 129.

Kliem, B. & Török, T. (2006), 'Torus Instability', *Physical Review Letters* **96**(25), 255002.

Kliem, B., Török, T. & Thompson, W. T. (2012), 'A Parametric Study of Erupting Flux Rope Rotation. Modeling the "Cartwheel CME" on 9 April 2008', *Solar Physics* **281**, 137–166.

Kuckein, C., Martínez Pillet, V. & Centeno, R. (2012*a*), 'An active region filament studied simultaneously in the chromosphere and photosphere. I. Magnetic structure', *Astronomy and Astrophysics Journal* **539**, A131.

Kuckein, C., Martínez Pillet, V. & Centeno, R. (2012*b*), 'An active region filament studied simultaneously in the chromosphere and photosphere. II. Doppler velocities', *Astronomy and Astrophysics Journal* **542**, A112.

Kuijpers, J. (1997), 'A Solar Prominence Model', *The Astrophysical Journal* **489**, L201.

Kumar, P., Cho, K.-S., Bong, S.-C., Park, S.-H. & Kim, Y. H. (2012), 'Initiation of coronal mass ejection and associated flare caused by helical kink instability observed by sdo/aia', *The Astrophysical Journal* **746**(1), 67.

Kuperus, M. (1996), 'The Double Inverse Polarity Paradigm—The Sign of Magnetic Fields in Quiescent Prominences', *Solar Physics* **169**, 349–356.

Kuperus, M. & Raadu, M. A. (1974), 'The Support of Prominences Formed in Neutral Sheets', *Astronomy and Astrophysics Journal* **31**, 189.

Kusano, K., Bamba, Y., Yamamoto, T. T., Iida, Y., Toriumi, S. & Asai, A. (2012), 'Magnetic Field Structures Triggering Solar Flares and Coronal Mass Ejections', *The Astrophysical Journal* **760**, 31.

Lang, K. R. (1999), *Astrophysical formulae*.

Leamon, R. J., Canfield, R. C., Blehm, Z. & Pevtsov, A. A. (2003), 'What Is the Role of the Kink Instability in Solar Coronal Eruptions?', *The Astrophysical Journal* **596**, L255–L258.

Lin, H., Penn, M. J. & Tomczyk, S. (2000), 'A New Precise Measurement of the Coronal Magnetic Field Strength', *The Astrophysical Journal* **541**, L83–L86.

Lin, J. & van Ballegooijen, A. A. (2005), 'Equilibrium and Evolution in Multipolar Magnetic Configurations Resulting from Interactions among Active Regions', *The Astrophysical Journal* **629**, 582–591.

Lin, R. P., Dennis, B. R., Hurford, G. J., Smith, D. M., Zehnder, A., Harvey, P. R., Curtis, D. W., Pankow, D., Turin, P., Bester, M., Csillaghy, A., Lewis, M., Madden, N., van Beek, H. F., Appleby, M., Raudorf, T., McTiernan, J., Ramaty, R., Schmahl, E., Schwartz, R., Krucker, S., Abiad, R., Quinn, T., Berg, P., Hashii, M., Sterling, R., Jackson, R., Pratt, R., Campbell, R. D., Malone, D., Landis, D., Barrington-Leigh, C. P., Slassi-Sennou, S., Cork, C., Clark, D., Amato, D., Orwig, L., Boyle, R., Banks, I. S., Shirey, K., Tolbert, A. K., Zarro, D., Snow, F., Thomsen, K., Henneck, R., McHedlishvili, A., Ming, P., Fivian, M., Jordan, J., Wanner, R., Crubb, J., Preble, J., Matranga, M., Benz, A., Hudson, H., Canfield, R. C., Holman, G. D., Crannell, C., Kosugi, T., Emslie, A. G., Vilmer, N., Brown, J. C., Johns-Krull, C., Aschwanden, M., Metcalf, T. & Conway, A. (2002), 'The Reuven Ramaty High-Energy Solar Spectroscopic Imager (RHESSI)', *Solar Physics* **210**, 3–32.

Lionello, R., Linker, J. A. & Mikić, Z. (2009), 'Multispectral Emission of the Sun During the First Whole Sun Month: Magnetohydrodynamic Simulations', *The Astrophysical Journal* **690**, 902–912.

Lionello, R., Riley, P., Linker, J. A. & Mikić, Z. (2005), 'The Effects of Differential Rotation on the Magnetic Structure of the Solar Corona: Magnetohydrodynamic Simulations', *The Astrophysical Journal* **625**, 463–473.

Lites, B. W., Kubo, M., Berger, T., Frank, Z., Shine, R., Tarbell, T., Title, A., Okamoto, T. J. & Otsuji, K. (2010), 'Emergence of Helical Flux and the Formation of an Active Region Filament Channel', *The Astrophysical Journal* **718**, 474–487.

Liu, R. & Alexander, D. (2009), 'Hard x-ray emission in kinking filaments', *The Astrophysical Journal* **697**(2), 999.

Liu, R., Kliem, B., Török, T., Liu, C., Titov, V. S., Lionello, R., Linker, J. A. & Wang, H. (2012), 'Slow Rise and Partial Eruption of a Double-decker Filament. I. Observations and Interpretation', *The Astrophysical Journal* **756**, 59.

Liu, Y. & Lin, H. (2008), 'Observational Test of Coronal Magnetic Field Models. I. Comparison with Potential Field Model', *The Astrophysical Journal* **680**, 1496–1507.

Low, B. C. (1994), 'Magnetohydrodynamic processes in the solar corona: Flares, coronal mass ejections, and magnetic helicity', *Physics of Plasmas* **1**, 1684–1690.

Low, B. C. & Observatory, H. A. (1996), '2 . The Large-Scale Corona Heating keeps the temperature of the corona in the million-degree range . The', pp. 217–265.

Lynch, B. J., Antiochos, S. K., MacNeice, P. J., Zurbuchen, T. H. & Fisk, L. A. (2004), 'Observable properties of the breakout model for coronal mass ejections', *The Astrophysical Journal* **617**(1), 589.

Mackay, D. H. & van Ballegooijen, A. A. (2006*a*), 'Models of the Large-Scale Corona. I. Formation, Evolution, and Liftoff of Magnetic Flux Ropes', *The Astrophysical Journal* **641**, 577–589.

Mackay, D. H. & van Ballegooijen, A. A. (2006*b*), 'Models of the Large-Scale Corona. II. Magnetic Connectivity and Open Flux Variation', *The Astrophysical Journal* **642**, 1193–1204.

Mackay, D. H. & Yeates, A. R. (2012), 'The Sun's Global Photospheric and Coronal Magnetic Fields: Observations and Models', *Living Reviews in Solar Physics* **9**, 6.

MacTaggart, D. & Hood, A. W. (2009*a*), 'Multiple eruptions from magnetic flux emergence', *Astronomy and Astrophysics Journal* **508**, 445–449.

MacTaggart, D. & Hood, A. W. (2009*b*), 'On the emergence of toroidal flux tubes: general dynamics and comparisons with the cylinder model', *Astronomy and Astrophysics Journal* **507**, 995–1004.

Magara, T. (2006), 'Dynamic and Topological Features of Photospheric and Coronal Activities Produced by Flux Emergence in the Sun', *The Astrophysical Journal* **653**, 1499–1509.

Manchester, W. B., Gombosi, T. I., Roussev, I., de Zeeuw, D. L., Sokolov, I. V., Powell, K. G., Tóth, G. & Opher, M. (2004), 'Three-dimensional MHD simulation of a flux rope driven CME', *Journal of Geophysical Research (Space Physics)* **109**, A01102.

Manchester, W. B., Gombosi, T. I., Roussev, I., Ridley, A., de Zeeuw, D. L., Sokolov, I. V., Powell, K. G. & Tóth, G. (2004), 'Modeling a space weather event from the Sun to the Earth: CME generation and interplanetary propagation', *Journal of Geophysical Research (Space Physics)* **109**, A02107.

Martínez González, M. J., Collados, M., Ruiz Cobo, B. & Beck, C. (2008), 'Internetwork magnetic field distribution from simultaneous 1.56 μm and 630 nm observations', *Astronomy and Astrophysics Journal* **477**, 953–965.

Marubashi, K. (1997), 'Interplanetary magnetic flux ropes and solar filaments', *Washington DC American Geophysical Union Geophysical Monograph Series* **99**, 147–156.

Metcalf, T. R., De Rosa, M. L., Schrijver, C. J., Barnes, G., van Ballegooijen, A. A., Wiegelmann, T., Wheatland, M. S., Valori, G. & McTtiernan, J. M. (2008), 'Nonlinear Force-Free Modeling of Coronal Magnetic Fields. II. Modeling a Filament Arcade and Simulated Chromospheric and Photospheric Vector Fields', *Solar Physics* **247**, 269–299.

Miller, J. A., Cargill, P. J., Emslie, A. G., Holman, G. D., Dennis, B. R., LaRosa, T. N., Winglee, R. M., Benka, S. G. & Tsuneta, S. (1997), 'Critical issues for understanding particle acceleration in impulsive solar flares', *Journal of Geophysical Research (Space Physics)* **102**, 14631–14660.

Mitalas, R. & Sills, K. R. (1992), 'On the photon diffusion time scale for the sun', *The Astrophysical Journal* **401**, 759.

Moffatt, H. K. (1969), 'The degree of knottedness of tangled vortex lines', *Journal of Fluid Mechanics* **35**, 117–129.

Moffatt, H. K. & Ricca, R. L. (1992), 'Helicity and the Calugareanu Invariant', *Proceedings of the Royal Society of London Series A* **439**, 411–429.

Moore, R. L., Sterling, A. C., Hudson, H. S. & Lemen, J. R. (2001), 'Onset of the Magnetic Explosion in Solar Flames and Coronal Mass Ejections', *the Astrophysical Journal,* **552**, 833–848.

Moreno-Insertis, F. (1997), 'Emergence of magnetic flux from the solar interior', **68**, 429.

Neukirch, T. (2005), Magnetic Field Extrapolation, *in* D. E. Innes, A. Lagg & S. A. Solanki, eds, 'Chromospheric and Coronal Magnetic Fields', Vol. 596 of *ESA Special Publication*, p. 12.1.

Okamoto, T. J., Tsuneta, S., Lites, B. W., Kubo, M., Yokoyama, T., Berger, T. E., Ichimoto, K., Katsukawa, Y., Nagata, S., Shibata, K., Shimizu, T., Shine, R. A., Suematsu, Y., Tarbell, T. D. & Title, A. M. (2008), 'Emergence of a Helical Flux Rope under an Active Region Prominence', *The Astrophysical Journal* **673**, L215.

Okamoto, T. J., Tsuneta, S., Lites, B. W., Kubo, M., Yokoyama, T., Berger, T. E., Ichimoto, K., Katsukawa, Y., Nagata, S., Shibata, K., Shimizu, T., Shine, R. A., Suematsu, Y., Tarbell, T. D. & Title, A. M. (2009), 'Prominence Formation Associated with an Emerging Helical Flux Rope', *The Astrophysical Journal* **697**, 913–922.

Owens, M. J. (2008), 'Combining remote and in situ observations of coronal mass ejections to better constrain magnetic cloud reconstruction', *Journal of Geophysical Research (Space Physics)* **113**, A12102.

Pagano, P., Mackay, D. H. & Poedts, S. (2013), 'Magnetohydrodynamic simulations of the ejection of a magnetic flux rope', *Astronomy and Astrophysics Journal* **554**, A77.

Parker, E. N. (1957*a*), 'Acceleration of cosmic rays in solar flares', *Physical Review* **107**, 830–836.

Parker, E. N. (1957*b*), 'The solar hydromagnetic dynamo', *Proceedings of the National Academy of Science* **43**, 8–14.

Parker, E. N. (1957*c*), 'Sweet's mechanism for merging magnetic fields in conducting fluids', *Journal of Geophysical Research (Space Physics)* **62**, 509–520.

Parker, E. N. (1958), 'Dynamics of the Interplanetary Gas and Magnetic Fields.', *The Astrophysical Journal* **128**, 664.

Parker, E. N. (1979*a*), *Cosmical magnetic fields: Their origin and their activity.*

Parker, E. N. (1979*b*), 'Sunspots and the physics of magnetic flux tubes. I - The general nature of the sunspot. II - Aerodynamic drag', *The Astrophysical Journal* **230**, 905–923.

Parker, E. N. (1996), 'The alternative paradigm for magnetospheric physics', *Journal of Geophysical Research (Space Physics)* **101**, 10587–10626.

Priest, E. (2014), *Magnetohydrodynamics of the Sun.*

Priest, E. R. (1982), *Solar magneto-hydrodynamics.*

Priest, E. R., van Ballegooijen, A. A. & Mackay, D. H. (1996), 'A Model for Dextral and Sinistral Prominences', *The Astrophysical Journal* **460**, 530.

Raadu, M. A. (1972), 'Suppression of the Kink Instability for Magnetic Flux Ropes in the Chromosphere', *Solar Physics* **22**, 425–433.

Riley, P., Linker, J. A., Mikić, Z., Lionello, R., Ledvina, S. A. & Luhmann, J. G. (2006), 'A Comparison between Global Solar Magnetohydrodynamic and Potential Field Source Surface Model Results', *The Astrophysical Journal* **653**, 1510–1516.

Riley, P., Lionello, R., Linker, J. A., Mikic, Z., Luhmann, J. & Wijaya, J. (2011), 'Global MHD Modeling of the Solar Corona and Inner Heliosphere for the Whole Heliosphere Interval', *Solar Physics* **274**, 361–377.

Romano, P., Contarino, L. & Zuccarello, F. (2003), 'Eruption of a helically twisted prominence', *Solar Physics* **214**, 313–323.

Rust, D. M. (2002), Magnetic helicity, coronal mass ejections and the solar cycle, *in* H. Sawaya-Lacoste, ed., 'Solspa 2001, Proceedings of the Second Solar Cycle and Space Weather Euroconference', Vol. 477 of *ESA Special Publication*, pp. 39–41.

Rust, D. M. & Kumar, A. (1994*a*), 'Helical magnetic fields in filaments', *Solar Physics* **155**, 69–97.

Rust, D. M. & Kumar, A. (1994*b*), Helicity charging and eruption of magnetic flux from the sun, *in* J. J. Hunt, ed., 'Solar Dynamic Phenomena and Solar Wind Consequences, the Third SOHO Workshop', Vol. 373 of *ESA Special Publication*, p. 39.

Scharmer, G. B., de la Cruz Rodriguez, J., Sütterlin, P. & Henriques, V. M. J. (2013), 'Opposite polarity field with convective downflow and its relation to magnetic spines in a sunspot penumbra', *Astronomy and Astrophysics Journal* **553**, A63.

Scherrer, P. H., Bogart, R. S., Bush, R. I., Hoeksema, J. T., Kosovichev, A. G., Schou, J., Rosenberg, W., Springer, L., Tarbell, T. D., Title, A., Wolfson, C. J., Zayer, I. & MDI Engineering Team (1995), 'The Solar Oscillations Investigation - Michelson Doppler Imager', *Solar Physics* **162**, 129–188.

Schmieder, B., Archontis, V. & Pariat, E. (2014), 'Magnetic Flux Emergence Along the Solar Cycle', *Space Science Reviews* **186**, 227–250.

Schmieder, B., Mein, N., Deng, Y., Dumitrache, C., Malherbe, J.-M., Staiger, J. & Deluca, E. E. (2004), 'Magnetic changes observed in the formation of two filaments in a complex active region: TRACE and MSDP observations', *Solar Physics* **223**, 119–141.

Schrijver, C. J., De Rosa, M. L., Metcalf, T. R., Liu, Y., McTiernan, J., Régnier, S., Valori, G., Wheatland, M. S. & Wiegelmann, T. (2006), 'Nonlinear Force-Free Modeling of Coronal Magnetic Fields Part I: A Quantitative Comparison of Methods', *Solar Physics* **235**, 161–190.

Schrijver, C. J., Title, A. M., Hagenaar, H. J. & Shine, R. A. (1997), 'Modeling the distribution of magnetic fluxes in field concentrations in a solar active region', *Solar Physics* **175**, 329–340.

Shafranov, V. D. (1958), 'On Magnetohydrodynamical Equilibrium Configurations', *Soviet Journal of Experimental and Theoretical Physics* **6**, 545.

Shafranov, V. D. (1966), 'Plasma Equilibrium in a Magnetic Field', *Reviews of Plasma Physics* **2**, 103.

Smith, E. J., Fillius, R. W. & Wolfe, J. H. (1978), 'Compression of Jupiter's magnetosphere by the solar wind', *Journal of Geophysical Research (Space Physics)* **83**, 4733–4742.

Solanki, S. K., Inhester, B. & Schüssler, M. (2006), 'The solar magnetic field', *Reports on Progress in Physics* **69**, 563–668.

Solanki, S. K., Lagg, A., Aznar Cuadrado, R., Orozco Suárez, D., Collados, M., Wiegelmann, T., Woch, J., Sasso, C. & Krupp, N. (2006), Measuring the Magnetic Vector with the He I 10830 Å Line: A Rich New World, *in* R. Casini & B. W. Lites, eds, 'Astronomical Society of the Pacific Conference Series', Vol. 358 of *Astronomical Society of the Pacific Conference Series*, p. 431.

Stenflo, J. O. (1973), 'Magnetic-Field Structure of the Photospheric Network', *Solar Physics* **32**, 41–63.

Stix, M. (1989), *The Sun. an Introduction.*

Sweet, P. A. (1958), 'The topology of force-free magnetic fields', *The Observatory* **78**, 30–32.

Taylor, J. B. (1974), 'Relaxation of Toroidal Plasma and Generation of Reverse Magnetic Fields', *Physical Review Letters* **33**, 1139–1141.

Titov, V. S. & Démoulin, P. (1999), 'Basic topology of twisted magnetic configurations in solar flares', *Astronomy and Astrophysics Journal* **351**, 707–720.

Török, T., Berger, M. A. & Kliem, B. (2010), 'The writhe of helical structures in the solar corona', *Astronomy and Astrophysics Journal* **516**, A49.

Török, T. & Kliem, B. (2003), 'The evolution of twisting coronal magnetic flux tubes', *Astronomy and Astrophysics Journal* **406**, 1043–1059.

Tousey, R. (1973), The solar corona., *in* M. J. Rycroft & S. K. Runcorn, eds, 'Space Research Conference', Vol. 2 of *Space Research Conference*, pp. 713–730.

Trujillo Bueno, J., Shchukina, N. & Asensio Ramos, A. (2004), 'A substantial amount of hidden magnetic energy in the quiet Sun', *Nature Physics* **430**, 326–329.

Trk, T. & Kliem, B. (2005), 'Confined and ejective eruptions of kink-unstable flux ropes', *The Astrophysical Journal Letters* **630**(1), L97.

Valori, G., Kliem, B. & Fuhrmann, M. (2007), 'Magnetofrictional Extrapolations of Low and Lou's Force-Free Equilibria', *Solar Physics* **245**, 263–285.

Valori, G., Kliem, B. & Keppens, R. (2005), 'Extrapolation of a nonlinear force-free field containing a highly twisted magnetic loop', *Astronomy and Astrophysics Journal* **433**, 335–347.

van Ballegooijen, A. A. (1999), 'Photospheric Motions as a Source of Twist in Coronal Magnetic Fields', *Washington DC American Geophysical Union Geophysical Monograph Series* **111**, 213–220.

van Ballegooijen, A. A. & Martens, P. C. H. (1989), 'Formation and eruption of solar prominences', *The Astrophysical Journal* **343**, 971–984.

van Ballegooijen, A. A., Priest, E. R. & Mackay, D. H. (2000), 'Mean Field Model for the Formation of Filament Channels on the Sun', *The Astrophysical Journal* **539**, 983–994.

Vásquez, A. M., Frazin, R. A., Hayashi, K., Sokolov, I. V., Cohen, O., Manchester, IV, W. B. & Kamalabadi, F. (2008), 'Validation of Two MHD Models of the Solar Corona with Rotational Tomography', *The Astrophysical Journal* **682**, 1328–1337.

Wang, Y. M., Nash, a. G. & Sheeley, N. R. (1989), *Magnetic flux transport on the sun.*, Vol. 245.

Wang, Y.-M. & Sheeley, Jr., N. R. (1994), 'The rotation of photospheric magnetic fields: A random walk transport model', *The Astrophysical Journal* **430**, 399–412.

Webb, D. F., Lepping, R. P., Burlaga, L. F., DeForest, C. E., Larson, D. E., Martin, S. F., Plunkett, S. P. & Rust, D. M. (2000), 'The origin and development of the May 1997 magnetic cloud', *Journal of Geophysical Research (Space Physics)* **105**, 27251–27260.

Wiegelmann, T. & Neukirch, T. (2002), 'Including stereoscopic information in the reconstruction of coronal magnetic fields', *Solar Physics* **208**, 233–251.

Wiegelmann, T. & Sakurai, T. (2012), 'Solar Force-free Magnetic Fields', *Living Reviews in Solar Physics* **9**, 5.

Williams, D. R., Török, T., Démoulin, P., van Driel-Gesztelyi, L. & Kliem, B. (2005), 'Eruption of a Kink-unstable Filament in NOAA Active Region 10696', *The Astrophysical Journal* **628**(2), L163–L166.

Wu, S. T., Zhang, T. X., Dryer, M., Feng, X. S. & Tan, A. (2005), 'The Role of Magnetic Reconnection in CME Acceleration', *Space Science Reviews* **121**, 33–47.

Yang, W. H., Sturrock, P. A. & Antiochos, S. K. (1986), 'Force-free magnetic fields - The magneto-frictional method', *The Astrophysical Journal* **309**, 383–391.

Yashiro, S., Gopalswamy, N., Michalek, G., St. Cyr, O. C., Plunkett, S. P., Rich, N. B. & Howard, R. A. (2004), 'A catalog of white light coronal mass ejections observed by the SOHO spacecraft', *Journal of Geophysical Research (Space Physics)* **109**, A07105.

Yurchyshyn, V. B., Wang, H., Goode, P. R. & Deng, Y. (2001), 'Orientation of the Magnetic Fields in Interplanetary Flux Ropes and Solar Filaments', *The Astrophysical Journal* **563**, 381–388.

Zirker, J. B., Martin, S. F., Harvey, K. & Gaizauskas, V. (1997), 'Global Magnetic Patterns of Chirality', *Solar Physics* **175**, 27–44.

Zurbuchen, T. H. & Richardson, I. G. (2006), 'In-Situ Solar Wind and Magnetic Field Signatures of Interplanetary Coronal Mass Ejections', *Space Science Reviews* **123**, 31–43.

List of Figures

4.19 (a) Plot showing the formation of a sigmoidal current sheet for the "incorrect" FR with a field line twist q = –1.25 rad a^{-1} scenario & (b) shows the magnitude of the current density across the y = 0 line. (c) Plot showing the formation of a sigmoidal current sheet for the "correct" FR with a field line twist q = –1.25 rad a^{-1} and (d) shows the magnitude of the current density in the y=0 line. 50

List of Tables